

Ab Initio Calculation of Relativistic Corrections to the Static Interquark Potential I: SU(2) Gauge Theory

Gunnar S. Bali*

*Physics Department, The University of Southampton
Highfield, Southampton SO17 1BJ, England*

Klaus Schilling[†], Armin Wachter[‡]

*HLRZ, Forschungszentrum Jülich, 52425 Jülich and
DESY, 22603 Hamburg, Germany*

and

*Fachbereich Physik, Bergische Universität, Gesamthochschule Wuppertal
Gaußstraße 20, 42097 Wuppertal, Germany*

(June 29, 2018)

Abstract

We test the capability of state-of-the-art lattice techniques for a precise determination of relativistic corrections to the static interquark potential, by use of SU(2) gauge theory. Emphasis is put on the short range structure of the spin dependent potentials, with lattice resolution a ranging from $a \approx 0.04$ fm (at $\beta = 2.74$) down to $a \approx 0.02$ fm (at $\beta = 2.96$) on volumes of 32^4 and 48^4 lattice sites. We find a new short range Coulomb-like contribution to the spin-orbit potential V_1' .

11.15.Ha, 12.38.Gc, 12.38.Aw, 12.39.Pn

Typeset using REVTeX

*Electronic mail: bali@hep.ph.soton.ac.uk

†Electronic mail: schillin@theorie.physik.uni-wuppertal.de

‡Electronic mail: wachter@hlrserv.hlrz.kfa-juelich.de

I. INTRODUCTION

Quarkonia spectroscopy provides a wealth of information and thus constitutes an important observational window to the phenomenology of confining quark interactions. It has been known for a long time that purely phenomenological or QCD inspired potential models offer a suitable heuristic framework to understand the empirical charmonium (J/ψ) and bottomonium (Υ) spectra [1–3].

On a more fundamental level, one would prefer to start out from the basic QCD Lagrangian to solve the heavy quarkonia bound state problem. Two alternative strategies lend themselves for reaching this goal: (i) direct extraction of the bound states on the lattice from an *effective nonrelativistic* lattice Lagrangian approximation (NRQCD) [4], (ii) use of an effective nonrelativistic Hamiltonian framework through the intermediary of potentials determined from lattice QCD.

Considerable efforts have been made recently to determine the quarkonia spectra within the NRQCD approximation of QCD [5]; the notorious technical problems to determine excited states in the Euclidean formulation have been tackled with remarkable success. In the alternative Schrödinger-Pauli setting, the technical problems are shifted towards the lattice determination of $1/m^2$ corrections to the potential. The spin dependent (sd) [6,7] and velocity dependent (vd) [8] contributions need to be extracted from (Euclidian) time asymptotia of rather complex observables that require renormalization and must obey constraints following from Lorentz symmetry [9,8].

First attempts to compute the relativistic corrections to the static potential on the lattice have been pioneered in the mid eighties [10–13]. In the meantime tremendous improvements have been achieved both in computational power and methods. The central potential has been determined with high accuracy in quenched QCD [14–16] and, more recently, in full QCD with two dynamical flavors of light Wilson sea quarks [17]. In view of the general interest in the potential formulation of the meson binding problem, renewed effort should be made to unravel the structure of sd and vd potentials. This will provide us with a better understanding of the structure of the interaction in the intermediate distance regime $0.15 \text{ fm} < r < 1 \text{ fm}$ which is of tantamount importance to the binding problem.

As a first step within this program we shall present in this paper a high statistics study of the spin dependent forces in SU(2) gauge theory. Though the two color formulation will not yet allow to proceed to spectrum calculations we would expect the key features of gluodynamical confinement to be revealed. In a follow-up paper [18] (referred to as II) we shall apply our techniques to the SU(3) case.

The present article is organized as follows: in Section II, we provide an introduction into the Hamiltonian formulation of QCD binding problems, the expected theoretical scenario of potentials as well as the lattice observables from which to determine them. In Section III, useful lattice techniques will be elaborated. In particular we shall discuss the systematic uncertainties of the approach. The resulting SU(2) gauge potentials will be presented in Section IV.

II. THE HEAVY QUARK POTENTIAL

A. Hamiltonian formulation of the meson binding problem

Starting from a Foldy-Wouthuysen transformation of the Euclidean quark propagator in an external gauge field, the asymptotic ($T \rightarrow \infty$) expression $\langle W(R, T) \rangle \propto \exp(-\hat{V}_0(R)T)$ for expectation values of Wilson loops can be derived. $V_0(r) = a^{-1}\hat{V}_0(R)$ denotes the potential between static quarks, separated by a distance $r = aR$. R and T are the spatial and temporal extents of the (rectangular) Wilson loop. By perturbing the propagator in terms of the inverse quark masses m_1^{-1} and m_2^{-1} around its static solution, one arrives at the semi-relativistic Hamiltonian (in the CM system, i.e. $\mathbf{p} = \mathbf{p}_1 = -\mathbf{p}_2$ and $\mathbf{L} = \mathbf{L}_1 = \mathbf{L}_2$),

$$H = \sum_{i=1}^2 \left(m_i + \frac{p^2}{2m_i} - \frac{p^4}{8m_i^3} \right) + V_0(r) + V_{\text{sd}}(r, \mathbf{L}, \mathbf{S}_1, \mathbf{S}_2) + V_{\text{vd}}(r, \mathbf{p}), \quad (1)$$

where the potential consists of a central part, sd [6,7] and vd [8] corrections¹,

$$\begin{aligned} V_{\text{sd}}(r, \mathbf{L}, \mathbf{S}_1, \mathbf{S}_2) = & \left(\frac{\mathbf{L}\mathbf{S}_1}{m_1^2} + \frac{\mathbf{L}\mathbf{S}_2}{m_2^2} \right) \frac{V_0'(r) + 2V_1'(r)}{2r} \\ & + \frac{\mathbf{L}(\mathbf{S}_1 + \mathbf{S}_2)}{m_1 m_2} \frac{V_2'(r)}{r} + \frac{S_1^i S_2^j}{m_1 m_2} \left(R_{ij} V_3(r) + \frac{\delta_{ij}}{3} V_4(r) \right) \end{aligned} \quad (2)$$

with

$$R_{ij} = \frac{r_i r_j}{r^2} - \frac{\delta_{ij}}{3} \quad (3)$$

and

$$\begin{aligned} V_{\text{vd}}(r, \mathbf{p}) = & \frac{1}{8} \left(\frac{1}{m_1^2} + \frac{1}{m_2^2} \right) \left(\nabla^2 V_0(r) + \nabla^2 V_a(r) \right) \\ & - \frac{1}{m_1 m_2} \{p_i, p_j, S_{ij}\}_{\text{Weyl}} + \sum_{k=1}^2 \frac{1}{m_k^2} \{p_i, p_j, T_{ij}\}_{\text{Weyl}} \end{aligned} \quad (4)$$

with $S_{ij} = \delta_{ij} V_b(r) - R_{ij} V_c(r)$ and $T_{ij} = \delta_{ij} V_d(r) - R_{ij} V_e(r)$. The symbol $\{\cdot, \cdot, \cdot\}_{\text{Weyl}} = \frac{1}{4} \{\cdot, \{\cdot, \cdot\}\}$ denotes Weyl ordering of the three arguments. $V_1' - V_4$ are related to spin-orbit and spin-spin interactions, $V_b - V_e$ to orbit-orbit interactions and the Darwin-like term that incorporates $\nabla^2 V_a$ modifies the central potential². $V_1' - V_4$ and $\nabla^2 V_a - V_e$ can be computed

¹ Here, we just state the classical values for the couplings to the potentials. Radiative corrections give rise to small deviations from these tree level results [19]. The corresponding one loop coefficients have recently been determined in the framework of heavy quark effective theory (HQET) in Ref. [20]. In the unequal mass case additional contributions appear, whose tree level coefficients are zero, that can also be parametrized in terms of V_1' and V_2' .

²In following the convention of Ref. [8] we have included this term into V_{vd} although it does not explicitly depend on the velocity.

from lattice correlation functions in Euclidean time of Wilson loop like operators. Pairs of the potentials are related by Lorentz invariance to the central potential [9,8]:

$$V_2'(r) - V_1'(r) = V_0'(r), \quad (5)$$

$$V_b(r) + 2V_d(r) = \frac{r}{6}V_0'(r) - \frac{1}{2}V_0(r), \quad (6)$$

$$V_c(r) + 2V_e(r) = -\frac{r}{2}V_0'(r), \quad (7)$$

such that only six sd and vd potentials turn out to be truly independent.

In the present SU(2) investigation, we restrict ourselves to the spin dependent terms. Note, that the Hamiltonian Eq. (1) contains dimension six operators and thus is not renormalizable. For this reason the theory — being truncated at order $1/m^2$ — is only an effective one with validity range of small gluon momenta (compared to the heavy quark masses). This very fact gave rise to a discrepancy between the Eichten-Feinberg-Gromes formulae Eq. (2) and perturbative expansions [21,19] in powers of the coupling, g , where additional logarithmic mass dependencies occurred from dimensional regularization. The underlying problem is now solved and one loop matching coefficients between the effective Hamiltonian and QCD have been obtained from HQET [20].

B. Expectations on sd potentials

In addition to the exact constraint, Eq. (5), derived by Gromes [9], some approximate relations between the sd potentials are anticipated from exchange symmetry arguments. We start from the standard assumption that the origin of the central potential is due to vector and scalar-like gluon exchange contributions. Given the fact that a vector-like exchange can at most grow logarithmically with r [22], the nature of the linear part of the confining potential can only be scalar. As we will see, $V_2'(r)$ is short ranged, such that the confining part only contributes to $V_1'(r)$. This leads us to expect $V_2'(r)$ to be purely vector-like. Under the additional assumptions that pseudoscalar contributions can be neglected and that V_1' does not contain a vector-like contributions, one ends up with the scenario of interrelations [9],

$$V_3(r) = \frac{V_2'(r)}{r} - V_2''(r), \quad (8)$$

$$V_4(r) = 2\nabla^2 V_2(r), \quad (9)$$

which of course has to be in agreement with leading order perturbation theory. However, Eqs. (8)–(9) hold true for any effective gluon propagator that transforms like a Lorentz vector. In principle, to this order in m^{-1} , V_3 and V_4 could contain additional pseudoscalar pieces.

Tree-level continuum perturbation theory (see Appendix) yields the following expectations for the central, spin-orbit and spin-spin potentials:

$$V_0(r) = -\frac{e}{r}, \quad (10)$$

$$V_1'(r) = 0, \quad (11)$$

$$V_2'(r) = \frac{e}{r^2}, \quad (12)$$

$$V_3(r) = \frac{3e}{r^3}, \quad (13)$$

$$V_4(r) = 8\pi e\delta^3(r), \quad (14)$$

where $e = C_F\alpha_s$ and $C_F = 3/4$ for SU(2). Note, that combining the perturbative result on $V_2'(r)$ with the Gromes relation, Eq. (5), and a funnel type parametrization of the central potential [1],

$$V_0(r) = -\frac{e}{r} + \kappa r, \quad (15)$$

the first spin-orbit potential should take the form

$$V_1'(r) = -\kappa. \quad (16)$$

In the Appendix we shall also derive the corresponding tree level results for the lattice potentials. We will show that an exact lattice relation between \tilde{V}_1' and \tilde{V}_2' and a linear combination of the central potential, taken at different lattice coordinates, in analogy to the Gromes relation does not exist. However, the relation should be retrieved in the continuum limit and approximately hold within the scaling region on the lattice.

C. How to compute the potentials

In the potential picture, the quarks interact instantaneously through a potential that only depends on the distance, spins, and velocities of the sources, Eqs. (1), (2) and (4). All time dependence has been separated and implicitly included into coefficient functions of various interaction terms, the so called sd and vd potentials. These can be computed by a non-perturbative integration over gluonic interactions. Therefore, the sd and vd potentials incorporate a summation over all possible interaction times, t . One obtains the following expressions in terms of expectation values in presence of a gauge field background for the sd potentials [6,7]³:

$$\frac{R_k}{R} \tilde{V}_1'(\mathbf{R}) = 2\epsilon_{ijk} \lim_{\tau \rightarrow \infty} \int_0^\tau dt t \langle \langle \hat{B}_i(\mathbf{0}, 0) \hat{E}_j(\mathbf{0}, t) \rangle \rangle_W, \quad (17)$$

$$\frac{R_k}{R} \tilde{V}_2'(\mathbf{R}) = \epsilon_{ijk} \lim_{\tau \rightarrow \infty} \int_0^\tau dt t \langle \langle \hat{B}_i(\mathbf{0}, 0) \hat{E}_j(\mathbf{R}, t) \rangle \rangle_W, \quad (18)$$

$$R_{ij} \tilde{V}_3(\mathbf{R}) = 2 \lim_{\tau \rightarrow \infty} \int_0^\tau dt \left[\langle \langle \hat{B}_i(\mathbf{0}, 0) \hat{B}_j(\mathbf{R}, t) \rangle \rangle_W \right. \\ \left. - \frac{\delta_{ij}}{3} \langle \langle \hat{\mathbf{B}}(\mathbf{0}, 0) \hat{\mathbf{B}}(\mathbf{R}, t) \rangle \rangle_W \right], \quad (19)$$

$$\tilde{V}_4(\mathbf{R}) = 2 \lim_{\tau \rightarrow \infty} \int_0^\tau dt \langle \langle \hat{\mathbf{B}}(\mathbf{0}, 0) \hat{\mathbf{B}}(\mathbf{R}, t) \rangle \rangle_W. \quad (20)$$

³We have put the expressions into a form that is more suitable for lattice simulations. Via spectral decompositions of the underlying correlation functions, equality of the expressions to those of Refs. [6,7] can easily be shown.

With $a \rightarrow 0$, the above potentials should approach their continuum counterparts and rotational invariance should be restored, $\tilde{V}'_1(\mathbf{R}) = a^2 V'_1(aR)$, $\tilde{V}'_2(\mathbf{R}) = a^2 V'_2(aR)$, $\tilde{V}_3(\mathbf{R}) = a^3 V_3(aR)$ and $\tilde{V}_4(\mathbf{R}) = a^3 V_4(aR)$.

The operator $\langle\langle F_1 F_2 \rangle\rangle_W$ is defined as follows:

$$\langle\langle F_1 F_2 \rangle\rangle_W = \frac{\langle \text{Tr } \mathcal{P} [\exp (i g \int_{\partial W} dx_\mu A_\mu) F_1 F_2] \rangle}{\langle \text{Tr } \mathcal{P} [\exp (i g \int_{\partial W} dx_\mu A_\mu)] \rangle}, \quad (21)$$

where ∂W denotes a closed path (the contour of a Wilson loop $W(\mathbf{R}, T)$). \mathcal{P} denotes path ordering of the arguments. Following Ref. [13] we have chosen the following discretized version of Eq. (21) for the case of two color field insertions:

$$\langle\langle \hat{F}_1 \hat{F}_2 \rangle\rangle_W = - \frac{\langle \mathcal{P} [W(\Pi_1 - \Pi_1^\dagger)(\Pi_2 - \Pi_2^\dagger)] \rangle \langle W \rangle}{\langle \mathcal{P} [W(\Pi_1 + \Pi_1^\dagger)] \rangle \langle \mathcal{P} [W(\Pi_2 + \Pi_2^\dagger)] \rangle}, \quad (22)$$

where the subscripts 1 and 2 represent the multi-indices (n_1, μ_1, ν_1) and (n_2, μ_2, ν_2) , respectively. n_i are integer valued four-vectors. The above ratio of “eared” Wilson loops is visualized in Fig. 1. In order to avoid imaginary phases and factors $g^2 a^4$ from Eqs. (17)–(20), we use the following conventions for the electric and magnetic fields:

$$\hat{F}_{\mu\nu} = g a^2 F_{\mu\nu} \quad , \quad \hat{E}_i = \hat{F}_{i4} \quad , \quad \hat{B}_i = \frac{1}{2} \epsilon_{ijk} \hat{F}_{jk}. \quad (23)$$

In what follows, we have chosen $\Pi_{\mu\nu}(n)$ to be the average of the four plaquettes, enclosing the lattice point n ,

$$\Pi_{\mu\nu}(n) = \frac{1}{4} [P_{\mu,\nu}(n) + P_{\mu,\nu}(n) + P_{-\mu,-\nu}(n) + P_{-\mu,\nu}(n)] \quad (24)$$

with

$$P_{\mu,\nu}(n) = U_\mu(n) U_\nu(n + \hat{\mu}) U_\mu^\dagger(n + \hat{\nu}) U_\nu^\dagger(n) \quad , \quad U_{-\mu}(n) = U_\mu^\dagger(n - \hat{\mu}). \quad (25)$$

This choice of Π makes Eq. (22) correct up to order a^2 , the discretization error of the Wilson action, used for generating the gauge field background.

In practical computation, the temporal extent T of the Wilson loop W within Eqs. (17)–(20) is adapted according to the formula $T = t + 2\Delta t$. We choose to keep the minimal distance, Δt , between the “ears” and the spatial closures of the Wilson loop fixed. Note, that, strictly speaking, Eqs. (17)–(20) apply for the limit $\Delta t \rightarrow \infty$. Our coordinates are such that the Wilson loop $W(\mathbf{R}, t + 2\Delta t)$ extends from $n_4 = -\Delta t$ to $n_4 = t + \Delta t$ into the temporal direction and from $\mathbf{n} = \mathbf{0}$ to $\mathbf{n} = \mathbf{R}$ into the spatial directions. Physically speaking, Δt represents the time we allow the gluon field to decay into the ground state, after (before) creation (annihilation) of the $q\bar{q}$ -state. Hence this deexcitation time must be considered as an important control parameter of our measurements.

III. LATTICE SIMULATIONS

A. Simulation parameters

Since, apart from V'_1 , all sd potentials are expected to be short ranged, we will focus our attention onto short distance properties, i.e. aim at the smallest lattice resolution possible on our computers. The present simulations have been performed on $V = L_\sigma^3 L_\tau = 16^4, 32^4$ and 48^4 lattices at $\beta = 2.74$ and $\beta = 2.96$ which correspond to lattice spacings $a \approx 0.041$ fm and $a \approx 0.022$ fm, respectively (Table I). The number of independent Monte Carlo configurations n_{conf} , generated at each set of parameters, is included into the Table. The above physical scales have been adjusted such that the string tension comes out to be $4\sqrt{\kappa} = 440$ MeV. Using such small physical volumes, finite size effects (FSEs) have to be investigated. This will be done by comparing results obtained on a 16^4 lattice with 32^4 results at $\beta = 2.74$. Finite lattice resolution (i.e. finite a) effects are investigated by relating results, obtained at the two different values of the coupling.

B. Updating algorithm

The numerical calculations are performed on lattices with hypercubic geometry and periodic boundary conditions in all four directions. Throughout the simulation the standard Wilson action

$$S_W = -\beta \sum_{n, \mu > \nu} \frac{1}{2} \text{Tr} P_{\mu, \nu}(n) \quad (26)$$

with $\beta = 4/g^2$ has been used.

For the updating of the gauge fields, a hybrid of heatbath and overrelaxation algorithms has been implemented [23]. The Fabricius-Haan heatbath sweeps [24] have been randomly mixed with the overrelaxation step with probability 1/14. The links have been visited in lexicographical ordering within hypercubes of 2^4 lattice sites, i.e. within each such hypercube, first all links pointing into direction $\hat{1}$ are visited site by site, then all links in direction $\hat{2}$ etc.. After at least 2000 heatbath thermalization sweeps, measurements are taken every 100 or 200 sweeps at $\beta = 2.74$ and $\beta = 2.96$, respectively, to ensure decorrelation. We find no signs of any autocorrelation effects between successive configurations within any of the measured observables.

C. Link integration

Statistical fluctuations have been reduced by “integrating out” temporal links that appear within the Wilson loops and the electric ears analytically, wherever possible. By “link integration” we mean the following substitution [25]:

⁴This scale can only provide a rough orientation as here we are simulating SU(2) gauge theory, not full QCD.

$$U_4(n) \longrightarrow W_4(n) = \frac{\int_{SU(2)} dU U e^{-\beta S_{n,4}(U)}}{\int_{SU(2)} dU e^{-\beta S_{n,4}(U)}} \quad (27)$$

with

$$S_{n,\mu}(U) = -\frac{1}{2} \text{Tr} \left(U F_\mu^\dagger(n) \right), \quad (28)$$

and

$$F_\mu(n) = \sum_{\nu \neq \mu} U_\nu(n) U_\mu(n + \hat{\nu}) U_\nu^\dagger(n + \hat{\mu}). \quad (29)$$

$W_4(n)$ is in general not an $SU(2)$ element anymore.

In this way, time-like links are replaced by the mean value they take in the neighborhood of the enclosing staples $F_4(n)$. Only those links that do not share a common plaquette can be integrated independently.

In case of $SU(2)$ gauge theory, $W_4(n)$ can be calculated analytically,

$$W_4(n) = \frac{I_2(\beta f_\mu(n))}{f_\mu(n) I_1(\beta f_\mu(n))} F_\mu(n), \quad (30)$$

where $f_\mu(n) = \sqrt{\det(F_\mu(n))}$. I_n denote the modified Bessel functions.

D. Smearing

In order to achieve a satisfying overlap between the quark-antiquark ground state and the state created by the spatial parts of the Wilson loop, we have applied a smearing procedure [26,27] by iteratively replacing each spatial link $U_i(n)$ within the Wilson loop, by a “fat” link,

$$U_i(n) \rightarrow N \left(\alpha U_i(n) + \sum_{j \neq i} U_j(n) U_i(n + \hat{j}) U_j^\dagger(n + \hat{i}) \right), \quad (31)$$

with the appropriate normalization N and free parameter α . We find satisfactory ground state enhancement with the parameter choice $n_{\text{iter}} = 150$ and $\alpha = 2$. In Fig. 2 the resulting central interquark potentials are displayed. In Fig. 3, the corresponding ground state overlaps $C_0(R)$ are shown as a function of the source separation at $\beta = 2.74$. As can be seen, all overlaps are well above 0.9.

E. Spectral decomposition

In this section we will discuss the control of excited state contributions at finite deexcitation time Δt . As explained above, the spatial transporters within the Wilson loops have been smeared to suppress such pollutions from the very beginning, allowing to work with moderate values of Δt . This is vitally important, as statistical errors increase with the size

of the Wilson loop. In practice, we have decided to keep Δt fixed at a value suited for sufficient deexcitation and to increase the temporal extent of the Wilson loop according to $T = t + 2\Delta t$, i.e. with the separation t between the two ears. We found $\Delta t = 2$ to be appropriate.

Previous authors [11,12] have replaced the integrals over interaction times by discrete sums. This results in cut-off errors due to the finiteness of τ as well as additional order a^2 integration errors. Both sources of systematic uncertainties can be significantly reduced by exploiting transfer matrix techniques. For illustration of such techniques we start from the static potential which can be computed from Wilson loops: at Euclidean time $t = 0$, a creation operator,

$$\Gamma_{\mathbf{R}}^\dagger = q(\mathbf{0})U(\mathbf{0} \rightarrow \mathbf{R})q^\dagger(\mathbf{R}) \quad (32)$$

with a gauge covariant transporter $U(\mathbf{0} \rightarrow \mathbf{R})$ is applied to the vacuum state $|0\rangle$. $q^\dagger(\mathbf{R})$ creates a heavy quark spinor at position \mathbf{R} . The $q\bar{q}$ pair is then propagated to $t = T$ by static Wilson lines in presence of the gauge field background, and finally annihilated by $\Gamma_{\mathbf{R}}$. A spectral decomposition of the Wilson loop exhibits the following behavior ($\mathcal{T} = e^{-aH}$ denotes the transfer matrix, $\mathcal{T}|n\rangle = e^{-aE_n}|n\rangle$):

$$\begin{aligned} P_W = \langle W(\mathbf{R}, T) \rangle &= \frac{\text{Tr} \left(\Gamma_{\mathbf{R}} \mathcal{T}^T \Gamma_{\mathbf{R}}^\dagger \mathcal{T}^{L_\tau - T} \right)}{\text{Tr} \left(\mathcal{T}^{L_\tau} \right)} \\ &= \frac{1}{\sum_m e^{-\hat{E}_m L_\tau}} \sum_{m,n} |\langle m | \Gamma_{\mathbf{R}} | n, \mathbf{R} \rangle|^2 e^{-\hat{V}_n(\mathbf{R})T} e^{-\hat{E}_m(L_\tau - T)} \\ &= \sum_n |d_n(\mathbf{R})|^2 e^{-\hat{V}_n(\mathbf{R})T} \times \left(1 + \mathcal{O} \left(e^{-E_1(L_\tau - T)} \right) \right) \end{aligned} \quad (33)$$

with

$$d_n(\mathbf{R}) = \langle 0 | \Gamma_{\mathbf{R}} | n, \mathbf{R} \rangle \quad , \quad C_n(\mathbf{R}) = |d_n(\mathbf{R})|^2. \quad (34)$$

$|n, \mathbf{R}\rangle$ is the n th eigenstate of a $q\bar{q}$ pair, separated by a distance \mathbf{R} . $|d_n(\mathbf{R})|^2$ takes a positive value, whenever such a state has a non-vanishing overlap to the creation operator $\Gamma_{\mathbf{R}}^\dagger$, applied to the vacuum. $|n\rangle$ is the n th pure glue eigenstate (glueball). $\hat{V}_n(\mathbf{R})$ denotes the n th excitation of the $q\bar{q}$ potential and the vacuum energy E_0 has been set to zero. E_1 is the mass gap, i.e. the mass of the A_1^+ glueball. Due to its heavy mass and $L_\tau \gg T$, such back-propagating terms can be neglected to high accuracy. The overlaps are normalized, $\sum_n C_n(\mathbf{R}) = 1$, such that a ground state overlap $C_0(\mathbf{R}) \approx 1$ implies $C_n(\mathbf{R}) \ll 1$ for all $n > 0$. $C_0(\mathbf{R})$ can be increased by optimizing the path combination $U(\mathbf{0} \rightarrow \mathbf{R})$ within the creation operator Eq. (32) (smearing).

Now, let us define the operators,

$$\mathcal{F}_i = q \frac{1}{2i} \left(\Pi_i - \Pi_i^\dagger \right) q^\dagger \quad , \quad \mathcal{G}_i = q \frac{1}{2} \left(\Pi_i + \Pi_i^\dagger \right) q^\dagger, \quad (35)$$

i.e. $q\Pi_i q^\dagger = \mathcal{G}_i + i\mathcal{F}_i$, for the chromo field insertions within the nominator and denominator of Eq. (22). $i = (\mathbf{n}_i, \mu_i, \nu_i)$ denotes the position of the insertion as well as the color field component. In the present case, \mathbf{n}_i either takes the position $\mathbf{0}$ or \mathbf{R} . Let

$$f_{mn}^i(\mathbf{R}) = \langle m, \mathbf{R} | \mathcal{F}_i | n, \mathbf{R} \rangle \quad , \quad g_{mn}^i(\mathbf{R}) = \langle m, \mathbf{R} | \mathcal{G}_i | n, \mathbf{R} \rangle. \quad (36)$$

Hermiticity of \mathcal{F}_i and \mathcal{G}_i implies $f_{mn}^{i*} = f_{nm}^i$ and $g_{mn}^{i*} = g_{nm}^i$.

A spectral decomposition of a Wilson loop, $W(\mathbf{R}, T)$ with ears \mathcal{F}_1 and \mathcal{F}_2 inserted at times $n_4 = 0$ and $n_4 = t$, respectively (The Wilson loop extends from $n_4 = -\Delta t$ to $n_4 = t + \Delta t$), yields (where we have neglected the back-propagation of pure glue states):

$$\begin{aligned} P_W^{12} &= -\frac{1}{4} \langle \mathcal{P} [W(\mathbf{R}, T) (\Pi_1 - \Pi_1^\dagger) (\Pi_2 - \Pi_2^\dagger)] \rangle \\ &= \frac{\text{Tr} \left(\Gamma \mathcal{T}^{\Delta t} \mathcal{F}_1 \mathcal{T}^t \mathcal{F}_2 \mathcal{T}^{\Delta t} \Gamma^\dagger \mathcal{T}^{L_\tau - T} \right)}{\text{Tr} (\mathcal{T}^{L_\tau})} \\ &= e^{-\hat{V}_0 T} \sum_{l, m, n} \text{Re} \left(d_l d_n^* f_{lm}^1 f_{mn}^2 \right) e^{-(\Delta \hat{V}_l + \Delta \hat{V}_n) \Delta t} e^{-\Delta \hat{V}_m t} \end{aligned} \quad (37)$$

with $\Delta \hat{V}_n = \hat{V}_n - \hat{V}_0$. For better readability, the \mathbf{R} dependence of $\Gamma_{\mathbf{R}}$, $\hat{V}_n(\mathbf{R})$, $d_n(\mathbf{R})$ as well as $f_{mn}^i(\mathbf{R})$ has been omitted from the above equation.

Next, let us investigate the behavior of the Wilson loops with one ear, appearing in the denominator of Eq. (22). For an insertion of \mathcal{G}_i at time $n_4 = 0$ or $n_4 = t$ we find,

$$\begin{aligned} Q_W^i &= \frac{1}{2} \langle \mathcal{P} [W(\mathbf{R}, T) (\Pi_i + \Pi_i^\dagger)] \rangle \\ &= \frac{\text{Tr} \left(\Gamma \mathcal{T}^{\Delta t} \mathcal{G}_i \mathcal{T}^{t + \Delta t} \Gamma^\dagger \mathcal{T}^{L_\tau - T} \right)}{\text{Tr} (\mathcal{T}^{L_\tau})} \\ &= e^{-\hat{V}_0 T} \sum_{m, l} \text{Re} \left(d_l d_m^* g_{lm}^i \right) e^{-(\Delta \hat{V}_l + \Delta \hat{V}_m) \Delta t} e^{-\Delta \hat{V}_m t}. \end{aligned} \quad (38)$$

In combining the above expressions we finally obtain ,

$$\langle \langle \hat{F}_1 \hat{F}_2 \rangle \rangle_W = \frac{P_W^{12} P_W}{Q_W^1 Q_W^2} = \sum_m D_m^{12} e^{-\Delta \hat{V}_m t} \times \left(1 + E_m^{12} e^{-\Delta \hat{V}_1 \Delta t} + \dots \right) \quad (39)$$

with

$$D_m^{12} = \frac{\text{Re} (f_{0m}^1 f_{m0}^2)}{g_{00}^1 g_{00}^2} \quad (40)$$

and

$$E_m^{12} = \frac{\text{Re} [(d_1/d_0) (f_{1m}^1 f_{m0}^2 + f_{0m}^1 f_{m1}^2)]}{\text{Re} (f_{0m}^1 f_{m0}^2)} - \frac{\text{Re} [(d_1/d_0) g_{10}^1]}{g_{00}^1} - \frac{\text{Re} [(d_1/d_0) g_{10}^2]}{g_{00}^2}. \quad (41)$$

Again, all constants are understood to depend on \mathbf{R} .

Note, that unwanted excited state contributions are suppressed by the ratio d_1/d_0 as well as by $e^{-\Delta \hat{V}_1 \Delta t}$. The smallest value of Δt that appears within an integral over interaction times will determine the reliability of the result. The bosonic string picture expectation is $\Delta \hat{V}_1(R) = \pi/R$ [28]. This has been qualitatively confirmed in numerical studies [29,30],

such that $\Delta t = 2$ yields an excited state suppression by a factor $\exp(-4\pi/R)$ for large R , in addition to the ratio d_1/d_0 .

The creation operator Γ^\dagger projects only onto states within the A_{1g} representation of the appropriate symmetry group D_{4h} [29]. The lowest continuum angular momentum to which it couples is $L = 0$. The hybrid ($L = 1$) state E_u is the next excitation. The combination of magnetic ears we use, applied to a $q\bar{q}$ state within the A_{1g} representation, results in a pure E_u state which has no overlap with A_{1g} , such that $D_0^{12} = 0$ within all correlation functions of interest, i.e. all correlators decay exponentially with Euclidean time t . This does not hold true for some of the vd potentials.

Unlike in the case of the central potential, where the sum of the (non-negative) overlap coefficients C_m is normalized to one, the D_m^{12} are not normalized and can be negative. However, due to invariance under time inversion, $\sum_m D_m^{12} = 0$ in case of V'_1 and V'_2 since the correlation function has to vanish at $t = 0$. In combining Eq. (39) with Eqs. (19) or (20), we obtain for \tilde{V}_3 or \tilde{V}_4 :

$$\tilde{V}_{3,4} \propto \sum_{m>0} \int_0^\infty dt D_m^{12} e^{-\Delta\hat{V}_m t} = \sum_{m>0} \frac{D_m^{12}}{\Delta\hat{V}_m} \quad (42)$$

with appropriate color field positions $\mathbf{n}_1 = \mathbf{0}$, $\mathbf{n}_2 = \mathbf{R}$ and components $\mu_1, \nu_1, \mu_2, \nu_2$. Eqs. (17) and (18) yield:

$$\tilde{V}'_{1,2} \propto \sum_{m>0} \int_0^\infty dt t D_m^{12} e^{-\Delta\hat{V}_m t} = \sum_{m>0} \frac{D_m^{12}}{(\Delta\hat{V}_m)^2}. \quad (43)$$

From the above formulae it is evident that not only eigenvalues of the transfer matrix but also amplitudes enter in the computation of the sd potentials, which illustrates where renormalization constants come in, which are effectively removed by the multiplication with $(g_{00}^1 g_{00}^2)^{-1}$ [Eq. (40)]. This factor originates from the denominator of Eq. (22). The parameters D_m^{12} and $\Delta\hat{V}_m$ can be fixed from a fit to Eq. (39). The hybrid potentials \hat{V}_m can in principle also be determined independently [29]. We leave this for future high precision studies on anisotropic lattices. For the time being, we evaluate the integrals Eqs. (17)–(20) numerically where our interpolation method has been inspired by the multi-exponential result of the spectral decomposition, Eq. (39).

F. Interpolation procedure

In order to determine the sd potentials, one must evaluate integrals over correlation functions [see Eqs. (17)–(20)] that depend on the interaction time t in a multi-exponential way, Eq. (39). In the following, $C_i(t)$ will denote the two point function which has to be integrated out in order to determine $\tilde{V}_i^{(l)}$ at a given value of \mathbf{R} . For $i = 1, 2$, $C_i(t)$ will be weighted by an additional factor t [Eqs. (17)–(18)]. Two different methods of interpolating $C_i(t)$ in between the discrete t -values have been adopted:

1. Wherever the quality of the signals allowed for reasonable fits, the data has been fitted to a two-exponential ansatz,

$$C(t) = D_1 \exp(-\Delta\hat{V}_1 t) + D_2 \exp(-\Delta\hat{V}_2 t). \quad (44)$$

This amounts to three parameter fits in case of C_1 and C_2 ($D_1 + D_2 = 0$) and four parameter fits for C_3 and C_4 . Unfortunately, stable fits have only been possible for the region of small R where we do not necessarily expect the hybrid potentials to agree with string model predictions.

2. Alternatively we have performed a local exponential interpolation:

$$C_i(t') = C_i(t) \exp[-B_i(t)(t' - t)] \quad , \quad B_i(t) = \ln \left(\frac{C_i(t)}{C_i(t+1)} \right) \quad (45)$$

for $t \leq t' < t + 1$ and $C_i(t)C_i(t+1) > 0$. Due to the multi-exponential character of the correlation function (or statistical fluctuations) the sign might change within the given interval. Thus, for $C_i(t)C_i(t+1) \leq 0$, we interpolate linearly,

$$C_i(t') = C_i(t) + [C_i(t+1) - C_i(t)](t' - t). \quad (46)$$

For $C_1(t)$ and $C_2(t)$ quadratical interpolations are performed within the interval $0 \leq t' < 1$ to account for $C_1(0) = C_2(0) = 0$, where we demand continuity of the interpolating function and its derivative at $t = 1$.

The interpolation procedure is illustrated in Figs. 4–7 for some examples. As can be seen from Fig. 4 where $C_1(t)$ is displayed for $R = 10$, the quadratic interpolation for $t < 1$ might differ significantly from the fit. However, this region does only weakly contribute to the potential since $C_1(t)$ as well as $C_2(t)$ are weighted by an additional factor t . In Figs. 5 and 6, $C_2(t)$ is displayed for $R = 2$ and $R = 4$, respectively. $C_4(t)$ at $R = 2$ changes its sign as can be seen from Fig. 7.

All statistical errors have been bootstrapped. For each potential $\tilde{V}_i^{(l)}$, numerical integration has been performed up to a value $t = \tau_i$, with τ_i chosen such that the result is stable (within statistical accuracy) under the replacement $\tau_i \rightarrow \tau_i - 1$ for all \mathbf{R} . Subsequently, systematic cut-off errors have been estimated from the exponential tail of fits to large t data points but came out to be negligible in all cases when compared to the statistical error from the numerical integration up to τ_i . Whenever the deviations between the fit and interpolation results turned out to be significant (see e.g. Fig. 7), we have included them as a systematic uncertainty into the final error on the potential value.

G. Renormalization and matching

The sd and vd potentials are computed from amplitudes of correlation functions rather than from eigenvalues of the transfer matrix. This gives rise to renormalizations in respect to the corresponding continuum potentials. A different way to illustrate the necessity of renormalization is the fact that the color electric (magnetic) ears,

$$\hat{F}_{\mu\nu} = ga^2 F_{\mu\nu} = \frac{1}{2i} \left(\Pi_{\mu\nu} - \Pi_{\mu\nu}^\dagger \right) \left(1 + \mathcal{O}(a^2) \right), \quad (47)$$

explicitly depend on the lattice scale a and, therefore, discretization.

As in the low energy regime of interest the renormalization constants are likely to receive relevant high order corrections, we apply the non-perturbative HM renormalization prescription [13] [cf. Eq. (22) and Fig. 1] that is geared to “dividing out” the two amplitudes g_{00}^1 and g_{00}^2 [Eqs. (40), (36)] from the naive lattice two point function. Terms that do not depend on a dimensionful parameter (which is the distance between the sources, R , in the case of interest) will give rise to divergencies in the continuum limit. The idea behind the HM procedure is to systematically remove such terms from the correlation functions in order to arrive at residual renormalization constants that are close to one.

In terms of perturbation theory, one can classify the related diagrams into pure self interactions within the ears, pure interactions within the Wilson loops, interactions between ears and the loop and — to higher orders — mixes thereof. By our renormalization procedure all divergent diagrams that consist only of ear or Wilson loop self interactions, cancel identically. In addition, many more complicated contributions are removed. Within $V_2' - V_4$, all divergencies of orders g^6 and less vanish while in case of V_1' this holds only true up to order⁵ g^4 , such that the renormalization constants involved will only differ from identity on a three loop [$1 + \mathcal{O}(g^6)$] or two loop [$1 + \mathcal{O}(g^4)$] level, respectively.

The spirit of the procedure is close to the one of Lepage-Mackenzie who suggest to construct “tadpole improved” operators [31]. In fact, one finds the HM renormalization and the tadpole improvement prescriptions to render near-equal results (within 2 %, as compared to overall renormalization effects of 60 %, at our present β -values). The remaining difference between the “tadpole improved” operator and the HM renormalized counterpart can be explained in terms of more complicated diagrams involving interactions between the ears and the time-like parts of the Wilson loop. We take the small size of this difference as an indication that other similar higher order terms, which we have not been able to cancel out completely, can be neglected.

Direct numerical checks of the accuracy of the approach are possible in two ways, namely (i) by varying the lattice resolution a and testing scaling of the results⁶ and (ii) by comparing the data with the prediction on $V_2' - V_1'$ from the Gromes relation, Eq. (5), between spin-orbit potentials and the central potential (which does not undergo renormalization),

$$V_0'(r) = V_{2,\text{ren}}'(r) - V_{1,\text{ren}}'(r). \quad (48)$$

In Fig. 8 we check our data on $V_2' - V_1'$ in units of the string tension κ against the force, obtained from a fit to the central potential, $V_0(r)$ [Eq. (51), Table II]. As can be seen, the two data sets scale beautifully onto each other and reproduce the central force up to lattice artefacts at small r .

⁵Within \tilde{V}_1' , gluon exchanges between the two ears that are not cancelled by the denominator of Eq. (22) contribute to the self energy.

⁶However, due to the running of the matching constants to the full theory with the lattice scale, residual scaling violations of about 2.7 % for V_1' , and V_2' and 5.5 % for V_3 and V_4 are expected after having rescaled the potentials by relative factors as large as $a_{2.74}^2/a_{2.96}^2 \approx 3.2$ and $a_{2.74}^3/a_{2.96}^3 \approx 5.7$, respectively. Needless to say, that we cannot resolve such tiny effects from our lattice data.

Renormalization is not a pure lattice problem in this case. By truncating the $1/m$ expansion of the SU(2) Lagrangian at a given order, the ultra-violet behavior is altered in respect to the full theory. Therefore, the resulting effective Lagrangian has to be matched to full SU(2) gauge theory at a renormalization scale $\mu = \pi/a$ giving rise to coefficients $c_i(\mu, m)$, connecting an SU(2) potential at the heavy quark mass m , $V_i(r; m)$ to the corresponding potential, computed in the framework of the effective theory at scale μ , e.g. $V_i(r; m) = c_i(\mu, m)V_i(r; \mu)$. This problem, which becomes visible beyond the tree-level, has been treated in a systematic manner for sd potentials by Chen *et al.* [20]. The Gromes relation still remains valid [$V_0'(r) = V_2'(r; \mu) - V_1'(r; \mu)$], and constrains the matching coefficients whose one loop values have been derived in the Reference. Unlike the renormalization constants that relate the lattice potentials to the continuum counterparts, in this case, we can rely on perturbative results, with the one loop correction being an effect of just a few per cent.

H. Finite volume effects

It is well known from previous simulations of SU(2) gauge theory (cf. Ref. [26]) that finite size effects (FSEs) on the central potential, computed from Wilson loops, and the string tension are negligible within the numerical accuracy of typical lattice studies, as long as the spatial lattice extent is kept larger than $L_\sigma \approx 1$ fm (and $L_\tau \geq L_\sigma$). However, since the critical temperature of the deconfinement phase transition corresponds to a scale of about 0.65 fm [32], the slope of the potential decreases rapidly as the extent of the box is reduced below about 0.8 fm. Nonetheless, one might expect the sd potentials $V_2' - V_4$ to be affected much less by the infrared cut-off than the central potential, as they are of much shorter range than the latter [see Eqs. (10), (12)–(14) or Eqs. (A37)–(A40) of the Appendix].

All results at $\beta = 2.74$ have been obtained on a volume of 32^4 lattice sites which is comfortably large. In addition, we have performed simulations on a 16^4 lattice, whose physical extent approximately corresponds to that of a 32^4 lattice at $\beta = 2.96$ (Table I), to estimate FSEs on the individual potentials. At $\beta = 2.96$, we have determined the string tension and parametrization of the central potential on a 48^4 lattice which is sufficiently large to avoid serious FSEs. The extracted scale $a = 0.022$ fm is in agreement with the expectation we have from the data collected in Ref. [26]. As expected, we find significant FSEs on the central potential obtained on a 32^4 lattice at this β -value as can be seen from Fig. 9. The slope is reduced by about 35 % on the small volume while the string tension on a 16^4 lattice at $\beta = 2.74$ comes out to be smaller by as much as 50 %, compared to $V = 32^4$.

At $\beta = 2.96$, the computer memory forced us to restrict ourselves to the smaller volume ($V = 32^4$) for the sd potentials. In the following, we compare results obtained on the 16^4 lattice to $V = 32^4$ results at $\beta = 2.74$ to justify the assumption that the $\beta = 2.96$ sd potentials are not seriously affected by FSEs. As can be seen from Figs. 10–13, for all sd potentials FSEs are statistically insignificant. Differences between the constant long range contributions to \tilde{V}'_1 , which we do expect, are hidden within the large statistical errors of the $\langle\langle B_i(\mathbf{0}, 0)E_j(\mathbf{0}, t) \rangle\rangle_W$ correlators. We conclude that though a spatial lattice extent of 0.7 fm is too small to extract the infinite volume central potential, it suffices for extracting $\tilde{V}'_2 - \tilde{V}'_4$ as well as the short distance contribution to \tilde{V}'_1 .

IV. PHYSICS RESULTS

A. Getting started: the central potential

The lattice potential data $\hat{V}_0(\mathbf{R})$ has been computed from smeared Wilson loops by the method described in Ref. [26]. Our general strategy is to derive continuous parametrizations of the lattice data points which will enable us to construct derivatives and compare the results to theoretical expectations, such as the exact Gromes relation [Eq. (5)] or the approximate relations, Eqs. (8)–(9). The continuum tree level results on the central and sd potentials have been presented in Section II B [Eqs. (10)–(14)] and the corresponding lattice expressions are derived in the Appendix [Eqs. (A6), (A31), (A23)–(A24) and (A20)], such that we can correct the lattice data for the differences before attempting to fit them to a continuous parametrization.

Let

$$\hat{V}_{\text{corr}}(R) = \hat{V}_0(\mathbf{R}) - g\delta\hat{V}_0(\mathbf{R}). \quad (49)$$

with

$$\delta\hat{V}_0(\mathbf{R}) = \frac{1}{R} - 4\pi G_L(\mathbf{R}) \quad (50)$$

be the tree level corrected central potential. The lattice gluon propagator $G_L(\mathbf{R})$ is defined in the Appendix [Eq. (A5)]. The lattice central potential can be fitted to the ansatz [including g of Eq. (49) as a fit parameter],

$$\hat{V}_{\text{corr}}(R) - \hat{V}_c = KR - \frac{e}{R} + \frac{\hat{f}}{R^2} - \frac{\hat{d}}{R^3} \quad (51)$$

with self energy \hat{V}_c , string tension K and Coulomb coefficient e . The $1/R^2$ and $1/R^3$ functional form of the corrections that account for the running of the coupling is not meant to be physical but has just been introduced to effectively parametrize the data within the given range of R -values. For the $\beta = 2.74$ data we have set $\hat{d} = 0$, such that we have 5 fit parameters in this case while we allow for 6 parameters at $\beta = 2.96$. The resulting parameter values are displayed in Table II. For technical reasons (link integration), only potential values for $R \geq \sqrt{2}$ have been obtained, such that the fits do not include $R = 1$.

In Fig. 2, the potentials $\hat{V}_{\text{corr}} - \hat{V}_c$ from both β -values are displayed in units of the string tension, K , as extracted from the fits, together with a fit curve that corresponds to the (averaged) values of fit parameters $e = 0.257$, $f = a\hat{f} = 0.0054/\sqrt{\kappa}$ and $d = a^2\hat{d} = 0.00011/\kappa$. As can be seen, the two data sets scale nicely onto each other which means that the result applies to the continuum. Violations of rotational invariance are removed by our correction method, even at very small values of R , and the data is well described by the parametrization over the whole r range.

B. Spin dependent Potentials

Our results on the first spin-orbit potential V_1' are displayed in Fig. 14 (in units of the string tension). The two data sets show approximate scaling behavior. In addition to a

constant long range contribution $-K$ as expected from Eq. (16), we find an attractive short range contribution that can be fitted to a Coulomb-like ansatz,

$$\tilde{V}'_1(r) = -\frac{h}{R^2} - K. \quad (52)$$

For these one parameter fits we have constrained the constant long range part to the value of the string tension, as obtained from the central potential. We find the values $h = 0.0474$ (58) and $h = 0.0439$ (23) at $\beta = 2.74$ and $\beta = 2.96$ for this dimensionless parameter, respectively. Averaging these two numbers yields $h = 0.0458$ (25). This additional term comes out unexpected⁷ and amounts to about one fifth of the e/r contribution to the central potential.

Taking into account the running coupling improved effective parametrization of the central potential [Eq. (51)] and the Gromes relation, we expect

$$V'_2(r) = \frac{e-h}{r^2} - \frac{2f}{r^3} + \frac{3d}{r^4} \quad (53)$$

as opposed to the tree level expectation Eq. (12). The Coulomb coupling has to be reduced by the amount that goes into V'_1 .

If we assume V'_1 to be generated exclusively from scalar-like exchanges and neglect the possibility of pseudoscalar contributions to V_3 , Eq. (8) leads us to modify Eq. (13) and expect,

$$V_3(r) = \frac{3(e-h)}{r^3} - \frac{8f}{r^4} + \frac{15d}{r^5}. \quad (54)$$

In Figs. 15 and 16, the spin-orbit potential V'_2 and the spin-spin potential V_3 are displayed, together with the expectations Eqs. (53) and (54), respectively. In both cases, we observe reasonable agreement between data and expectations. For small values of R , scaling violations between the two data sets from the different β -values are evident as well as (in case of V_3) some deviations from the expectation. As we will see in Section IV C, these differences can be explained as finite a effects and understood in terms of lattice perturbation theory.

In Fig. 17, the spin-spin potential \tilde{V}_4 is displayed in lattice units for the two β -values. An oscillatory behavior is observed which is similar to that of the lattice δ -function, expected on the tree level [Eq. (A20) of the Appendix]. Moreover, the two data sets nearly coincide with each other, in distinct violation of scaling. Higher order corrections to the δ -function which might scale with an appropriate dimension should account for the differences between the two data sets at small R .

⁷However, from the results of Ref. [20] and the Gromes relation, we can derive the following one loop connection between results on $V'_1(r; \mu_i)$, obtained at lattice spacings $a_1 = \pi/\mu_1$ and $a_2 = \pi/\mu_2$ [18]: $V'_1(r; \mu_2) = V'_1(r; \mu_1) - \left(1 - (\alpha(\mu_2)/\alpha(\mu_1))^{9/25}\right) V'_2(r; \mu_1)$, which means (i) that such a contribution must exist and (ii) that its relative weight will increase with decreasing lattice spacing. However, the actual magnitude of this admixture is still surprising as the prefactor of the admixture from V'_2 is as small as about 0.03 under a scale change by a factor two.

C. Finite a aspects

In Figs. 18–20, we focus on the small R behavior of the sd potentials $\tilde{V}'_2, \tilde{V}_3$ and \tilde{V}_4 . We restrict ourselves to display the $\beta = 2.74$ results only which are in qualitative agreement with those obtained at $\beta = 2.96$. In addition to the data (with error bars), the tree level perturbative expressions from the Appendix are displayed [squares, Eq. (A31) for \tilde{V}'_2 , Eqs. (A23) and (A24) for \tilde{V}_3 and Eq. (A20) for \tilde{V}_4]. The normalization constants $c = C_F \alpha_s$ have been obtained from fits to the first seven data points. All three sd potentials are qualitatively described by these one parameter fits and deviations of the data from a continuous curve can be understood in terms of this lattice expectation.

The fit parameters are displayed in Table III. From the analysis of the central potential, we would expect values $c = e - h \approx 0.21$ while the tree level lattice expectations [with lattice coupling $\alpha_s = 1/(\pi\beta)$] are $c = 0.087$ and $c = 0.081$ for $\beta = 2.74$ and $\beta = 2.96$, respectively. In agreement with the perturbative expectation, all c_i come out to decrease with increasing β . We find $c = e - h$ as determined from V_0 and V'_1 to be about 2.5 times larger than the naive tree level value while this factor reduces to 1.8 in case of \tilde{V}'_2 and 1.3 for \tilde{V}_3 and \tilde{V}_4 as these potentials are dominated by higher momentum gluon exchanges and thus more perturbative. In order to investigate if the remaining differences between data points and tree level expectation (with renormalized coupling c_i as fit parameters) can be explained in terms of higher order perturbative corrections, we attempt to model running coupling effects.

The only additional diagrams that contribute to V_0 at $\mathcal{O}(g^4)$ on the lattice as well as in the continuum are one loop corrections to the gluon self energy. The renormalization of the coupling, emanating from these diagrams, has been computed on the lattice for on-axis separations of the sources [33,34]. One can account for this correction by building in a running coupling constant $\alpha(\mathbf{q})$ into the gluon propagator in momentum space [Eq. (A5)]. Instead of attempting to compute the correct lattice sum, we model this effect by the corresponding continuum expression,

$$\alpha(t) = \frac{1}{4\pi b_0 t} \left(1 + \frac{b}{t} \ln t + \frac{b^2}{t^2} \ln t \right)^{-1} \quad (55)$$

with

$$t = \ln \left(\frac{\hat{q}^2}{\Lambda^2} \right) \quad , \quad b_0 = \frac{11N}{48\pi^2} \quad , \quad b_1 = \frac{34N}{3(16\pi^2)^2} \quad , \quad b = \frac{b_1}{b_0^2}, \quad (56)$$

where we replace q^2 by its lattice counterpart $\hat{q}^2 = 4 \sum_i \sin^2(q_i/2)$ to account for the periodic boundary conditions. The case $b = 0$ corresponds to the one loop result. The difference to the correct lattice expression of Ref. [34] is small. Λ is a QCD scale parameter that can be related to the usual schemes via perturbation theory.

To $\mathcal{O}(g^6)$, apart from a renormalization of the gluon propagator, additional exchange contributions appear that can be resummed into a single running coupling by renormalization group arguments. These arguments do not apply to the lattice where rotational invariance is broken, such that, in addition to its absolute value, the direction of \mathbf{q} has to be taken into

account. Bearing this in mind, we will nonetheless attempt to model two loop effects by the continuum two loop running coupling of Eq. (55).

In case of the sd potentials V_2' – V_4 , not only the gluon self energy contributes to $\mathcal{O}(g^4)$ but also exchange diagrams between the ears, incorporating a three gluon vertex. In the continuum these can be resummed into an effective running coupling. Due to this resummation, the scale parameters Λ_i (for $V_i^{(l)}$) can differ from each other. Again, we attempt to model this effect by plugging the continuum running coupling at scales \hat{q} into the lattice tree level expressions.

In case of the sd potentials, the infrared region is suppressed by powers of q [Eqs. (A38)–(A40)], such that the form of the propagator in the non-perturbative domain has little effect. To remove the unphysical pole at $q = \Lambda$, an infrared protection can be build in into the propagator by substituting t by $t_c = \ln(q^2/\Lambda^2 + c^2)$ with a constant c . The smallest momentum on the finite lattice is $q = \pi/(aL_\sigma)$. We choose $c^2 = \max(0, e - \pi^2/(aL_\sigma\Lambda)^2)$ (e is the Euler constant) to guarantee $t \geq 1$ with c^2 being negligible at large momenta $q \approx 1/a$.

We do not attempt to fit the central potential to its perturbative expectation because this would require us to put a $1/q^4$ -like piece into the propagator by hand to generate the string tension. Also, as we found out, a large part of the short range structure is of scalar nature and would have to be modeled separately. A running coupling analysis of the central force in position space can be found in Refs. [15,16].

Fits of the one loop as well as the two loop running coupling improved expectations (with one free parameter Λ) to the first 4–8 data points of each potential have been performed. The results of the two loop fits to 7 data points are included into Figs. 18–20 (circles, dotted lines). The running coupling significantly improves agreement with the data. Differences between one and two loop results are small. The Λ parameters remain stable against the variation of the fit range within 10 %.

In Table III, results on the Λ parameters from our one and two loop fits are collected. We do not include any errors since the fits are only thought to qualitatively describe the data with reduced χ^2 -values of typically 10–100. We observe approximate scaling between the two sets of Λ parameters at $\beta = 2.74$ and $\beta = 2.96$ within 15 %. However, the two loop values are larger by about a factor two than the corresponding one loop values.

V. CONCLUSIONS AND OUTLOOK

We have devised methods to determine spin dependent interquark forces to high precision. From our high statistics lattice simulation in SU(2) gauge theory, we find reliable renormalized potentials with good scaling behavior. There is clear evidence for a short range scalar exchange contribution in the long range spin-orbit potential at the level of 20 % of the Coulomb part of the central potential. The other sd potentials are found to be short ranged and are well understood by means of perturbation theory.

An extension of the present investigations to the case of interest, SU(3) gauge theory, and inclusion of velocity dependent corrections will be presented in II [18]. As a further step, predictions from various models of QCD interactions, such as dual QCD [35] can be tested against lattice results on the potentials. Also spectra, wave functions and decay constants for arbitrary (sufficiently large) values of the quark masses can be computed just

by solving a simple differential equation [36]. Subsequently, these results can be confronted with experiment or compared to results from direct lattice NRQCD predictions [5] as a first principles check of the viability of the instantaneous approximation of the potential picture.

ACKNOWLEDGMENTS

During completion of this work GSB has been supported by EU grant ERB CHBG CT94-0665. We appreciate support by EU grants SC1*-CT91-0642 and CHRX-CT92-00551 as well as DFG grants Schi 257/1-4 and Schi 257/3-2.

APPENDIX A: WEAK COUPLING EXPANSION OF LATTICE POTENTIALS

In this appendix, we will elaborate the tree level expectations for the sd potentials from a weak coupling expansion of SU(N) gauge theory on the lattice. Some of these expressions have already been derived in Ref. [13] for on-axis source separations. To illustrate the method, we start with the central potential before considering sd corrections. We include the corresponding continuum expressions for completeness.

1. Central potential

A weak coupling expansion of the Wilson loop yields to lowest order in g^2 ,

$$\langle W(\mathbf{R}, T) \rangle = \exp \left(-C_F g^2 \frac{1}{2} \sum_{m,n,\mu,\nu} J_\mu(m) G(m-n) \delta_{\mu\nu} J_\nu(n) \right) \quad (\text{A1})$$

$$= \exp \left(C_F g^2 T \sum_{t=0}^{T-1} [G(\mathbf{R}, t) - G(\mathbf{0}, t)] \right) \quad (T \gg R) \quad (\text{A2})$$

where $J_\mu(m) = \pm 1$ if $(m, \mu) \in \partial W$ and $J_\mu(m) = 0$ elsewhere. Only terms, extensive in T , have been kept in Eq. (A2). For SU(2), the color factor $C_F = \frac{N^2-1}{2N}$ becomes $C_F = 3/4$. $G(n)$ denotes the lattice gluon propagator in position space,

$$G(n) = \frac{1}{L_\sigma^3 L_\tau} \sum_{q \neq 0} \frac{e^{iqn}}{\sum_\mu \hat{q}_\mu^2} \quad , \quad \hat{q}_\mu = 2 \sin \left(\frac{q_\mu}{2} \right) \quad (\text{A3})$$

with

$$\begin{aligned} q_i &= \frac{2\pi}{L_\sigma} m_i \quad , \quad m_i = -\frac{L_\sigma}{2} + 1, \dots, \frac{L_\sigma}{2}, \\ q_4 &= \frac{2\pi}{L_\tau} m_4 \quad , \quad m_4 = -\frac{L_\tau}{2} + 1, \dots, \frac{L_\tau}{2}. \end{aligned} \quad (\text{A4})$$

Note, that we have neglected the zero momentum contribution to W which is suppressed by a factor $RT/(L_\sigma^3 L_\tau)$.

With

$$G_L(\mathbf{R}) = \sum_t G(\mathbf{R}, t) = \frac{1}{L_\sigma^3} \sum_{\mathbf{q} \neq \mathbf{0}} \frac{e^{i\mathbf{q}\mathbf{R}}}{\sum_i \hat{q}_i^2} \quad (\text{A5})$$

and $\hat{V}_0(\mathbf{R}) = -\lim_{T \rightarrow \infty} \ln(W(\mathbf{R}, T))/T$, one obtains

$$\hat{V}_0(\mathbf{R}) = -C_F g^2 (G_L(\mathbf{R}) - G_L(\mathbf{0})) \longrightarrow \hat{V}_c - C_F \alpha_s \frac{1}{R} \quad (R \rightarrow \infty) \quad (\text{A6})$$

for the central potential with $\alpha_s = g^2/(4\pi)$. $\hat{V}_c = C_F g^2 G_L(\mathbf{0})$ denotes a self energy constant.

2. Spin-spin potentials

To compute $\tilde{V}'_1(\mathbf{R}) - \tilde{V}_4(\mathbf{R})$ from Eqs. (17) – (20), only gluon exchanges between the two color field insertions (ears) have to be considered to order g^2 . Starting from

$$\langle P_1 P_2 \rangle = \exp(-C_F g^2 X_{12}) \quad (\text{A7})$$

with

$$X_{12} = \sum_{m,n,\mu,\nu} J_\mu^1(m) G(m-n) \delta_{\mu\nu} J_\nu^2(n) \quad (\text{A8})$$

where $J_\mu^i(n) = \pm 1$ (the sign depends on the orientation of the link) if $(n, \mu) \in \partial P_i$ and $J_\mu^i(n) = 0$ elsewhere, we obtain to order g^2 [Eq. (22)],

$$\begin{aligned} \langle \langle \tilde{F}_1 \tilde{F}_2 \rangle \rangle_W &= - \frac{\langle \mathcal{P} [W (P_1 - P_1^\dagger)(P_2 - P_2^\dagger)] \rangle \langle W \rangle}{\langle \mathcal{P} [W (P_1 + P_1^\dagger)] \rangle \langle \mathcal{P} [W (P_2 + P_2^\dagger)] \rangle} \\ &= -\frac{1}{4} \langle (P_1 - P_1^\dagger)(P_2 - P_2^\dagger) \rangle \\ &= -\frac{1}{2} (\langle P_1 P_2 \rangle - \langle P_1 P_2^\dagger \rangle) \\ &= \sinh(C_F g^2 X_{12}) = C_F g^2 X_{12}, \end{aligned} \quad (\text{A9}) \quad (\text{A10})$$

with $\tilde{F}_j = \frac{1}{2i} (P_j - P_j^\dagger)$. Note, that the self energy contributions from interactions within one ear are not small, though of order g^4 , but a 60 % contribution at our β -values. However, such contributions are cancelled by the denominator of Eq. (A9). Within the potentials $\tilde{V}'_2 - \tilde{V}_4$, all order g^6 self interactions are cancelled as well.

Let us consider the correlation function between two magnetic ears at positions $(\mathbf{0}, 0)$ and (\mathbf{R}, t) where we choose the first ear to be within the $\hat{i} - \hat{j}$ plane and the latter within the $\hat{i} - \hat{k}$ plane with $i \neq j, i \neq k$. In this case, we obtain

$$V_{12} = 2 \int_0^\infty dt \langle \langle \tilde{F}_1 \tilde{F}_2 \rangle \rangle_W = -C_F g^2 (\Delta_j^{(-)} \Delta_k^{(+)} + \delta_{jk} \Delta_i^{(-)} \Delta_i^{(+)}) G_L(\mathbf{R}) \quad (\text{A11})$$

where

$$\Delta_i^{(+)} f(\mathbf{n}) = f(\mathbf{n} + \hat{\mathbf{i}}) - f(\mathbf{n}) \quad , \quad \Delta_i^{(-)} f(\mathbf{n}) = f(\mathbf{n}) - f(\mathbf{n} - \hat{\mathbf{i}}) \quad (\text{A12})$$

are forward/backward differences. Note, that

$$G_L(\mathbf{R}) = 2 \int_0^\infty dt G(\mathbf{R}, t). \quad (\text{A13})$$

Interactions between averages of four adjacent plaquettes centered around lattice points $\mathbf{0}$ and \mathbf{R} , which we use for the magnetic ears [Eq. (24)], can be derived from Eq. (A11) by averaging over the 16 possible combinations of single plaquette ears,

$$V_{12}^A = -C_F g^2 \left(\Delta_j^{(-)} \Delta_k^{(+)} + \delta_{jk} \Delta_i^{(-)} \Delta_i^{(+)} \right) \Xi_j^{(+)} \Xi_k^{(-)} \Xi_i G_L(\mathbf{R}) \quad (\text{A14})$$

$$= -C_F g^2 \left(\Delta_j \Delta_k \Xi_i + \delta_{jk} \Delta_i^2 \Xi_j \right) G_L(\mathbf{R}) \quad (\text{A15})$$

with

$$\Xi_i^{(+)} f(\mathbf{n}) = \frac{1}{2} \left(f(\mathbf{n}) + f(\mathbf{n} + \hat{\mathbf{i}}) \right), \quad (\text{A16})$$

$$\Xi_i^{(-)} f(\mathbf{n}) = \frac{1}{2} \left(f(\mathbf{n}) + f(\mathbf{n} - \hat{\mathbf{i}}) \right), \quad (\text{A17})$$

$$\Xi_i f(\mathbf{n}) = \frac{1}{4} \left(2f(\mathbf{n}) + f(\mathbf{n} + \hat{\mathbf{i}}) + f(\mathbf{n} - \hat{\mathbf{i}}) \right), \quad (\text{A18})$$

$$\Delta_i f(\mathbf{n}) = \frac{1}{2} \left(f(\mathbf{n} + \hat{\mathbf{i}}) - f(\mathbf{n} - \hat{\mathbf{i}}) \right). \quad (\text{A19})$$

Note, that $\Xi_i = \frac{1}{2}(\Xi_i^{(+)} + \Xi_i^{(-)}) = \Xi_i^{(+)} \Xi_i^{(-)}$, $\Xi_i \Xi_j = \frac{1}{2}(\Xi_i + \Xi_j)$, $\Delta_i = \frac{1}{2}(\Delta_i^{(+)} + \Delta_i^{(-)}) = \Delta_i^{(+)} \Xi_i^{(-)} = \Delta_i^{(-)} \Xi_i^{(+)}$. Since all Ξ and Δ are linear combinations of translations, they commute with each other.

In case of \tilde{V}_4 the two magnetic ears are parallel, i.e. $j = k$, such that a sum over the three possible i, j combinations [Eq. (20)] yields,

$$\tilde{V}_4(\mathbf{R}) = -2C_F g^2 \sum_{i=1}^3 \Delta_i^2 \Xi_i^{(\perp)} G_L(\mathbf{R}) = -2C_F g^2 \Delta^{(2)} \Xi G_L(\mathbf{R}) \quad (\text{A20})$$

with

$$\Xi_i^{(\perp)} = \frac{1}{2} \sum_{j \neq i} \Xi_j \quad , \quad \Xi = \frac{1}{3} \sum_i \Xi_i, \quad (\text{A21})$$

$$\Delta_i^{(2)} = \Delta_i^{(+)} \Delta_i^{(-)} \quad , \quad \Delta^{(2)} = \sum_i \Delta_i^{(2)}. \quad (\text{A22})$$

Note, that $\Delta_i^2 = \Delta_i^{(2)} \Xi_i$.

Correlators between B_l and B_m are required for computation of \tilde{V}_3 . Since the direction of \mathbf{B} is orthogonal to the plane of the corresponding plaquettes, we find the relations, $k = l$, $j = m$ and $i \neq j$, $i \neq k$ for $l \neq m$. In case (l, i, j) are cyclic, (m, i, k) are automatically anticyclic, such that we obtain an overall minus sign. We find for $j \neq k$ from Eq. (19)⁸,

⁸Obviously, this expression is only useful for off-axis separations where $R_j \neq 0$ and $R_k \neq 0$.

$$\frac{R_j R_k}{R^2} \tilde{V}_3(\mathbf{R}) = C_F g^2 \Delta_j \Delta_k \Xi_i G_L(\mathbf{R}). \quad (\text{A23})$$

For $l = m = i$ we obtain:

$$\begin{aligned} 3R_{ii} \tilde{V}_3 &= C_F g^2 \left(2\Delta_i^2 \Xi_i^{(\perp)} - \Delta_j^2 (2\Xi_k - \Xi_i) - \Delta_k^2 (2\Xi_j - \Xi_i) \right) G_L(\mathbf{R}) \\ &= C_F g^2 \frac{1}{2} \left(5\Delta_i^{(2)} \Xi - \Delta^{(2)} \Xi - \Delta_j^{(2)} \Xi_k - \Delta_k^{(2)} \Xi_j \right) G_L(\mathbf{R}) \end{aligned} \quad (\text{A24})$$

with $j \neq i, k \neq i, j \neq k, R_{ij} = R_i R_j / R^2 - \delta_{ij} / 3$.

It is easy to see that the above expressions amount to

$$V_4(r) = -2C_F \alpha_s \nabla^2 \frac{1}{r} = 8\pi C_F \alpha_s \delta^3(r) \quad (\text{A25})$$

and

$$V_3(r) = C_F \alpha_s \frac{r^2}{r_i r_j} \partial_i \partial_j \frac{1}{r} = 3C_F \alpha_s \frac{1}{r^3} \quad (\text{A26})$$

or

$$V_3(r) = C_F (R_{ii})^{-1} \frac{1}{3} \left(2\partial_i^2 - \partial_j^2 - \partial_k^2 \right) \frac{1}{r} = C_F \alpha_s (R_{ii})^{-1} \frac{3r_i^2 - r^2}{r^5} = 3C_F \alpha_s \frac{1}{r^3} \quad (\text{A27})$$

in the continuum limit.

3. Spin-orbit potentials

For computation of \tilde{V}'_1 and \tilde{V}'_2 one has to take into account correlators between plaquettes in the $\hat{i} - \hat{j}$ plane and the $\hat{i} - \hat{4}$ plane. To lowest order in g only exchanges between the links oriented in \hat{i} direction have to be taken into account. With

$$2 \int_0^\infty dt t [G(\mathbf{R}, t) - G(\mathbf{R}, t + 1)] = G_L(\mathbf{R}), \quad (\text{A28})$$

we obtain

$$W_{12} = \int_0^\infty dt t \langle \langle \tilde{F}_1 \tilde{F}_2 \rangle \rangle_W = -C_F g^2 \frac{1}{2} \Delta_i^{(-)} G_L(\mathbf{R}) \quad (\text{A29})$$

for the integrated correlation function. Averaging over the relevant plaquette combinations finally yields,

$$W_{12}^A = -C_F g^2 \frac{1}{2} \Delta_j \Xi_i G_L(\mathbf{R}). \quad (\text{A30})$$

Thus, \tilde{V}'_1 vanishes to order g^2 while the leading order expression for the second spin-orbit potential [Eq. (18)] is,

$$\tilde{V}'_2(\mathbf{R}) = -\frac{R}{R_j} C_F g^2 \Delta_j \Xi_j^{(\perp)} G_L(\mathbf{R}). \quad (\text{A31})$$

In the continuum this amounts to,

$$V'_2(r) = -C_F \alpha_s \frac{r}{r_j} \partial_j \frac{1}{r} = C_F \alpha_s \frac{1}{r^2}. \quad (\text{A32})$$

4. Tree level relations

Tree level relations between the lattice potentials that are analogous to Eqs. (5) and (9) can be derived:

$$\tilde{V}'_2(\mathbf{R}) = \frac{R}{R_j} \Delta_j \Xi_j^{(\perp)} \hat{V}_0(\mathbf{R}) + \tilde{V}'_1(\mathbf{R}), \quad (\text{A33})$$

$$\tilde{V}_4(\mathbf{R}) = 2\Delta_i^{(2)} \Xi \hat{V}_0(\mathbf{R}) = 2 \sum_i \Delta_i \left(\frac{R_i}{R} \tilde{V}'_2(\mathbf{R}) \right). \quad (\text{A34})$$

From Eq. (A33) one might attempt to generalize the Gromes relation. Let us assume for the moment that a linear difference operator exists, such that

$$\tilde{V}'_2(\mathbf{R}) - \tilde{V}'_1(\mathbf{R}) = \sum_{\mathbf{n}} c(\mathbf{n}) \hat{V}_0(\mathbf{R} + \mathbf{n}) \quad (\text{A35})$$

with constants $c(\mathbf{n})$. Both sides of the above equation can be expanded in orders of g^2 . At order g^2 we find,

$$\sum_{\mathbf{n}} c(\mathbf{n}) G_L(\mathbf{R} + \mathbf{n}) = \frac{R}{R_j} \Delta_j \Xi_j^{(\perp)} G_L(\mathbf{R}). \quad (\text{A36})$$

The factor R/R_j illustrates that $c(\mathbf{n})$ has to depend on \mathbf{R} , in contradiction to the ansatz, i.e. nonlinear corrections have to be included. Also, in our numerical studies we find the tree level relation Eq. (A33) to be substantially violated at small R . Of course, the continuum Gromes relation as well as the above lattice version are retrieved at large R .

5. Continuum results

For continuum potentials one obtains the following tree level expressions,

$$V_0(r) = -C_F \alpha_s \int \frac{dq^3}{2\pi^2} \frac{e^{i\mathbf{q}\mathbf{r}}}{q^2} = -C_F \frac{2\alpha_s}{\pi} \int_0^\infty dq \frac{\sin qr}{qr} = -C_F \frac{\alpha_s}{r}, \quad (\text{A37})$$

$$V'_2(r) = -iC_F \alpha_s \int \frac{dq^3}{2\pi^2} \frac{\mathbf{q}\mathbf{r}}{q^2 r} e^{i\mathbf{q}\mathbf{r}} = -C_F \frac{2\alpha_s}{\pi} \int_0^\infty dq q^2 r j_1(qr) = C_F \frac{\alpha_s}{r^2}, \quad (\text{A38})$$

$$V_3(r) = -C_F \alpha_s \int \frac{dq^3}{2\pi^2} \frac{(\mathbf{q}\mathbf{r})^2}{q^2 r^2} e^{i\mathbf{q}\mathbf{r}} = -C_F \frac{2\alpha_s}{\pi} \int_0^\infty dq q^2 j_2(qr) = 3C_F \frac{\alpha_s}{r^3}, \quad (\text{A39})$$

$$V_4(r) = C_F \alpha_s \int \frac{dq^3}{2\pi^2} e^{i\mathbf{q}\mathbf{r}} = C_F \frac{2\alpha_s}{\pi} \int_0^\infty dq q^2 \frac{\sin qr}{qr} = 8\pi C_F \alpha_s \delta^3(r). \quad (\text{A40})$$

A linear confining contribution can be introduced by adding a $1/q^4$ term to V_0 in momentum space. The integrals for the sd potentials are suppressed at low q like q^2 or q^3 , such that we naively expect perturbation theory to be more reliable in this case than for the ground state potential. Also, finite size effects are expected to be smaller. V'_1 vanishes at tree level.

REFERENCES

- [1] E. Eichten, K. Gottfried, T. Kinoshita, J. Kogut, K.D. Lane, and T.-M. Yan, Phys. Rev. Lett. **34**, 369 (1975).
- [2] C. Quigg, and J.L. Rosner, Phys. Rep. **56**, 167 (1979), and References therein.
- [3] D. Gromes, W. Lucha, and F.F. Schöberl, Phys. Rep. **200** 127 (1991), and References therein.
- [4] B.A. Thacker and G.P. Lepage, Phys. Rev. **D43**, 196 (1991).
- [5] See e.g., C.T.H. Davies, K. Hornbostel, G.P. Lepage, A.J. Lidsey, J. Shigemitsu, and J. Sloan, Phys. Lett. **B382**, 131 (1996).
- [6] E. Eichten and F. Feinberg, Phys. Rev. Lett. **43**, 1205 (1979); Phys. Rev. **D23**, 2724 (1981).
- [7] D. Gromes, Z. Phys. **C22**, 265 (1984).
- [8] A. Barchielli, E. Montaldi, and G.M. Prosperi, Nucl. Phys. **B296**, 625 (1988), Erratum: Nucl. Phys. **B303**, 752 (1988); A. Barchielli, N. Brambilla, and G.M. Prosperi, Nuovo Cimento **103A**, **N.1**, 59 (1990).
- [9] D. Gromes, Z. Phys. **C26**, 401 (1984).
- [10] C. Michael and P.E.L. Rakow, Nucl. Phys. **B256**, 640 (1985); C. Michael, Phys. Rev. Lett. **56**, 1219 (1986).
- [11] M. Campostrini, K. Moriarty, and C. Rebbi, Phys. Rev. Lett. **57**, 44 (1986); Phys. Rev. **D36**, 3450 (1987).
- [12] P. de Forcrand and J.D. Stack, Phys. Rev. Lett. **55**, 1254 (1985).
- [13] A. Huntley and C. Michael, Nucl. Phys. **B286**, 211 (1987).
- [14] G.S. Bali and K. Schilling, Phys. Rev. **D46**, 2636 (1992); J. Mod. Phys. **C4**, 1167 (1993).
- [15] G.S. Bali and K. Schilling, Phys. Rev. **D47**, 661 (1993).
- [16] S.P. Booth, D.S. Henty, A. Hulsebos, A.C. Irving, C. Michael, and P.W. Stephenson, Phys. Lett. **B294** 385 (1992).
- [17] SESAM collaboration: U. Glässner, S. Güsken, H. Hoerber, T. Lippert, G. Ritzenhöfer, K. Schilling, G. Siegert, A. Spitz and A. Wachter, Phys. Lett. **B383**, 98 (1996).
- [18] G.S. Bali, K. Schilling and A. Wachter, Southampton preprint SHEP 96/28, in preparation.
- [19] J. Pantaleone, S.-H.H. Tye and Y.J. Ng, Phys. Rev. **D33**, 777 (1986).
- [20] Y.-Q. Chen, Y.-P. Kuang, and R.J. Oakes, Phys. Rev. **D52**, 264 (1995).
- [21] S.N. Gupta, S.F. Radford, and W.W. Repko, Phys. Rev. **D26** 3305 (1982); S.N. Gupta and S.F. Radford, Phys. Rev. **D25** 3430 (1982).
- [22] D. Gromes, Phys. Lett. **B202**, 262 (1988).
- [23] F.R. Brown and T.J. Woch, Phys. Rev. Lett. **28**, 2394 (1987); R. Gupta, G.W. Kilcup, A. Patel, S.R. Sharpe, and P. de Forcrand, Mod. Phys. Lett. **A3**, 1367 (1988).
- [24] K. Fabricius and O. Haan, Phys. Lett. **B143**, 459 (1984); A. Kennedy and B. Pendleton, Phys. Lett. **B156**, 393 (1985).
- [25] G. Parisi, R. Petronzio, and F. Rapuano, Phys. Lett. **128B**, (1983) 418.
- [26] G.S. Bali, K. Schilling, and C. Schlichter, Phys. Rev. **D51**, 5165 (1995).
- [27] APE Collaboration: M. Albanese *et al.*, Phys. Lett. **B192**, 163 (1987).
- [28] M. Lüscher, K. Symanzik, and P. Weisz, Nucl. Phys. **B173**, 365 (1980).

- [29] S. Perantonis, A. Huntley, and C. Michael, Nucl. Phys. **B326**, 544 (1989), and References therein.
- [30] A.M. Green, C. Michael, and P.S. Spencer, hep-lat/9610011, to be published in Phys. Rev. **D55**, (1997).
- [31] G.P. Lepage and P.B. Mackenzie, Phys. Rev. **D48**, (1993) 2250; see also: G. Parisi, Proceedings of the xxth International Conference on High Energy Physics 1980, Madison, Eds. L. Durand and L.G. Pondrom, American Institute of Physics, New York (1981) 1531.
- [32] J. Fingberg, U.M. Heller, and F. Karsch, Nucl. Phys. **B392**, 493 (1993); G.S. Bali, J. Fingberg, U.M. Heller, F. Karsch, and K. Schilling, Phys. Rev. Lett. **71**, 3059 (1993).
- [33] H. Kawai, R. Nakayama, and K. Seo, Nucl. Phys. **B189**, 40 (1981); A. DiGiacomo and G. Paffuti, Nucl. Phys. **B205**, 313 (1982).
- [34] U.M. Heller and F. Karsch, Nucl. Phys. **B258**, 29 (1985).
- [35] M. Baker, J.S. Ball, N. Brambilla, G.M. Prosperi and F. Zachariasen, Phys. Rev. **D54**, 2829 (1996); M. Baker, J.S. Ball, and F. Zachariasen, Phys. Rev. **D51**, 1968 (1995); Phys. Rep. **209**, 73 (1991).
- [36] G.S. Bali, K. Schilling, and A. Wachter, “Spin and velocity dependent corrections to the interquark potential and quarkonia spectra from Lattice QCD”, to be published in proceedings of “Quark confinement and the hadron spectrum (Confinement 96)”, Como, Italy, hep-ph/9611226; G.S. Bali, K. Schilling, and A. Wachter, in preparation.

TABLES

TABLE I. Simulation parameters. The physical scale has been obtained from $\sqrt{\kappa} = 440$ MeV.

β	$V = L_\sigma^3 L_\tau$	a/fm	L_σ/fm	n_{conf}
2.74	16^4	0.041	0.65	1290
2.74	32^4	0.041	1.30	200
2.96	32^4	0.022	0.70	204
2.96	48^4	0.022	1.05	67

TABLE II. Fit parameters to the central potential [Eqs. (49)–(51)].

Parameter	$\beta = 2.74$	$\beta = 2.96$	Average value
K	0.00785(13)	0.00246 (8)	—
e	0.2611(35)	0.2507(41)	0.2567(74)
\hat{f}	0.0598(33)	0.1114(76)	$0.00541(38)/\sqrt{K}$
\hat{d}	—	0.0437(50)	$0.000108(12)/K$
\hat{V}_c	0.4898(12)	0.4334 (9)	—
g	0.1707(12)	0.1409 (9)	—

TABLE III. The tree level constants $c = C_F \alpha_s$ and Λ parameters from the running coupling analysis of V'_2 , V_3 and V_4 .

tree level	c_2	c_3	c_4
$\beta = 2.74$	0.17	0.12	0.13
$\beta = 2.96$	0.14	0.10	0.11
running α	$\Lambda_2/\sqrt{\kappa}$	$\Lambda_3/\sqrt{\kappa}$	$\Lambda_4/\sqrt{\kappa}$
1-loop $\beta = 2.74$	0.29	0.12	0.08
1-loop $\beta = 2.96$	0.25	0.10	0.07
2-loop $\beta = 2.74$	0.67	0.32	0.20
2-loop $\beta = 2.96$	0.61	0.29	0.18

FIGURES

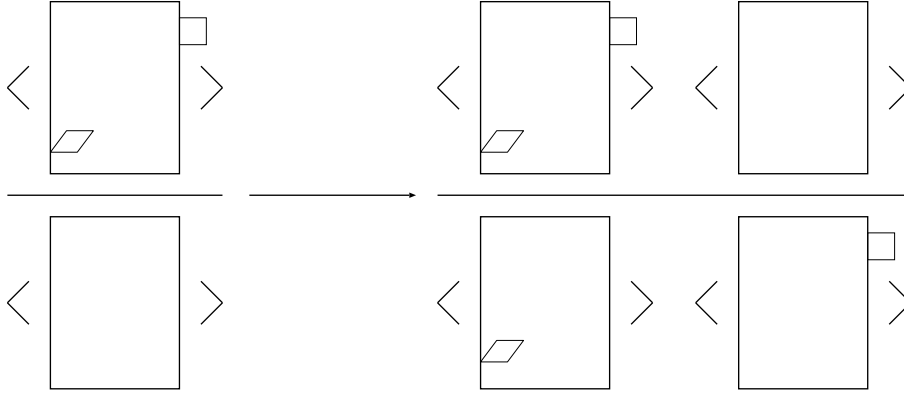


FIG. 1. Nonperturbative renormalization prescription for eared Wilson loops.

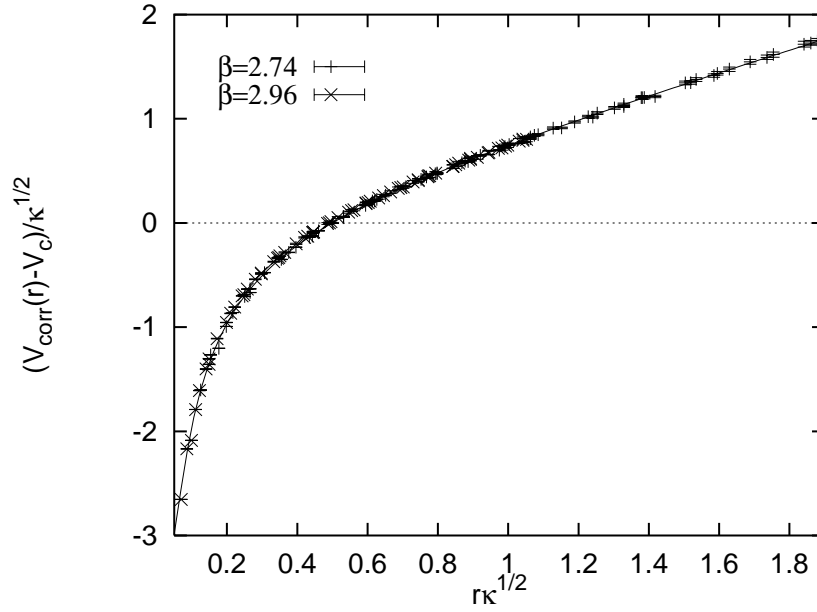


FIG. 2. Corrected central potential $V_{\text{corr}} - V_c$ in units of the string tension at $\beta = 2.74$ and $\beta = 2.96$. The fit curve corresponds to the parametrization Eq. (51) with parameter values as in the last column of Table II.

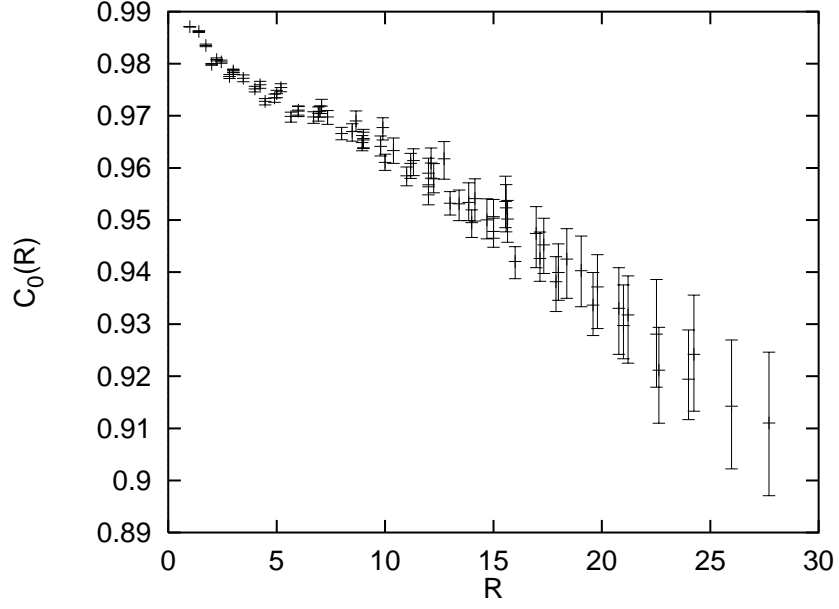


FIG. 3. Ground state overlaps as a function of the quark separation R (in lattice units) at $\beta = 2.74$.

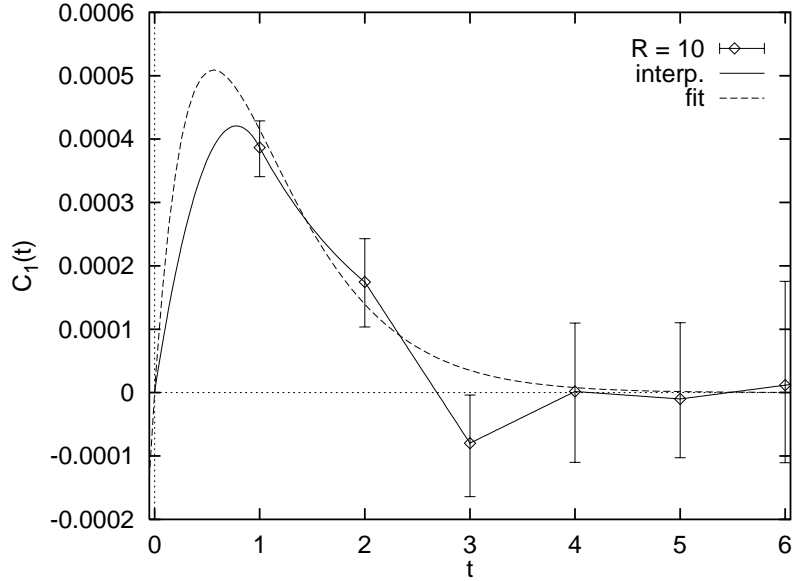


FIG. 4. The correlation function $C_1(t)$ for $R = 10$. The solid curve denotes our interpolation while the dashed curve corresponds to a three parameter fit to the data.

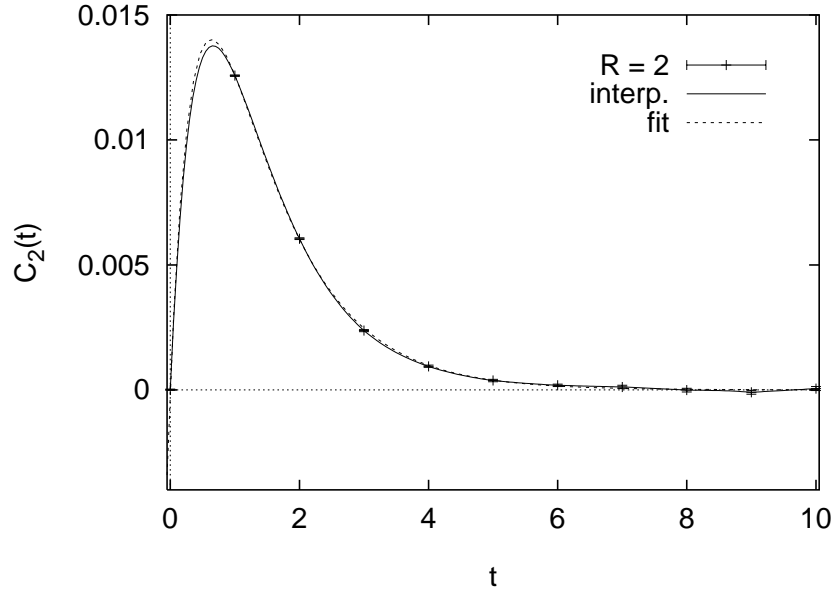


FIG. 5. The correlation function $C_2(t)$ for $R = 2$. The solid curve denotes our interpolation while the dashed curve corresponds to a three parameter fit to the data.

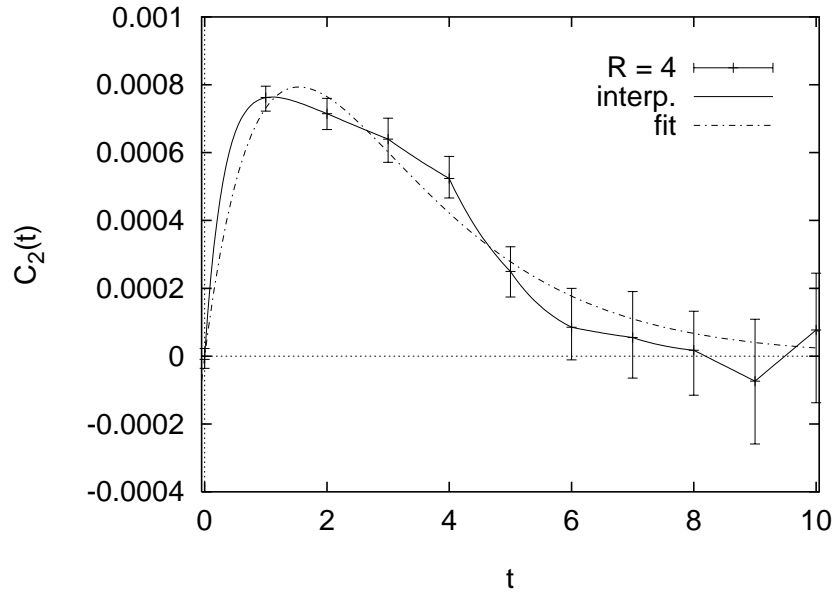


FIG. 6. The correlation function $C_2(t)$ for $R = 4$. The solid curve denotes our interpolation while the dashed-dotted curve corresponds to a three parameter fit to the data.

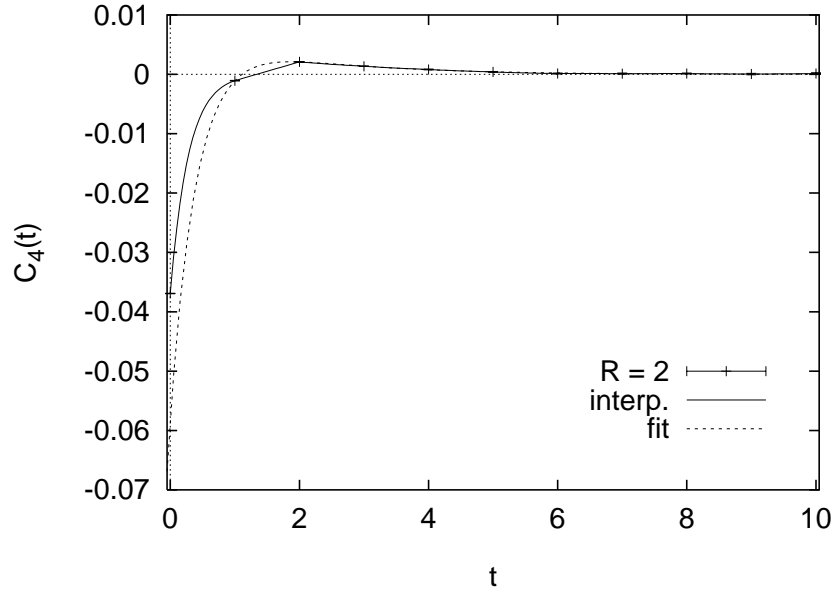


FIG. 7. The correlation function $C_4(t)$ for $R = 2$. The solid curve denotes our interpolation while the dashed curve corresponds to a four parameter fit to the data.

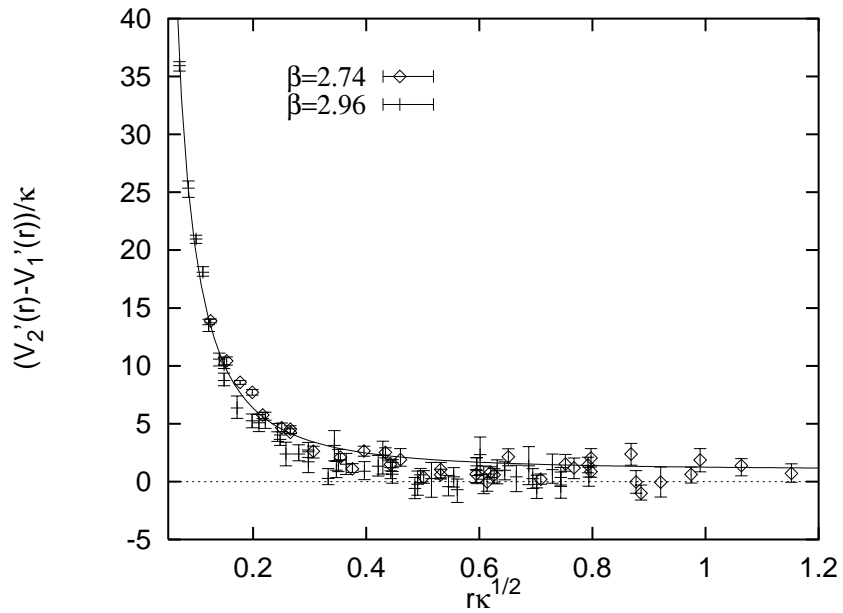


FIG. 8. Test of the Gromes relation Eq. (5). The combination $V_2' - V_1'$ is compared to the central force as obtained from the parametrization Eq. (51).

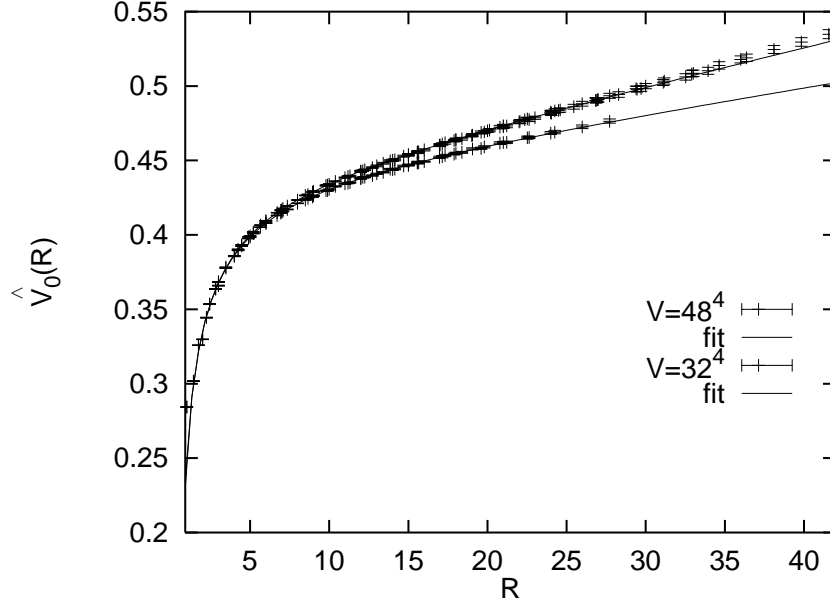


FIG. 9. Comparison of the central potential $\hat{V}_0(R)$ at $\beta = 2.96$ between a 32^4 and a 48^4 lattice (in lattice units).

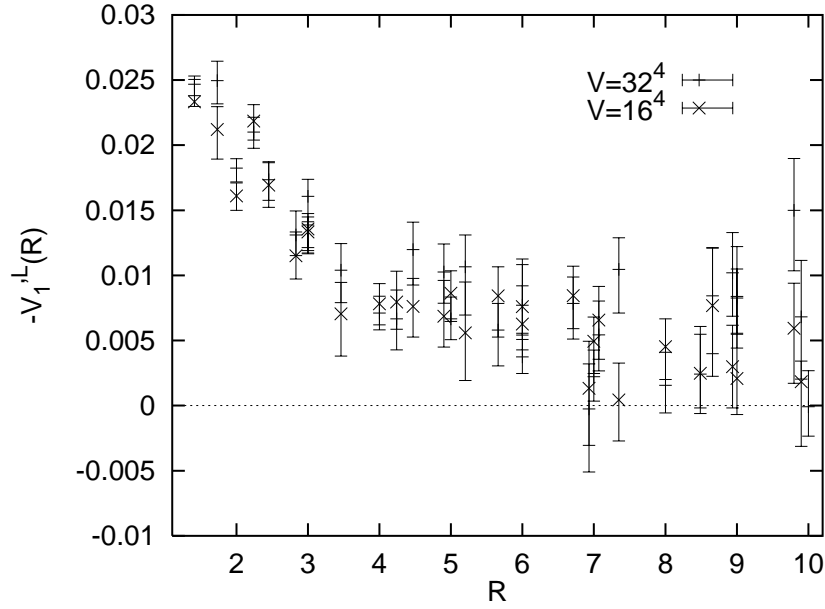


FIG. 10. Comparison between $-\tilde{V}'_1(R)$ at $\beta = 2.74$ obtained on a 16^4 lattice and a 32^4 lattice (in lattice units).

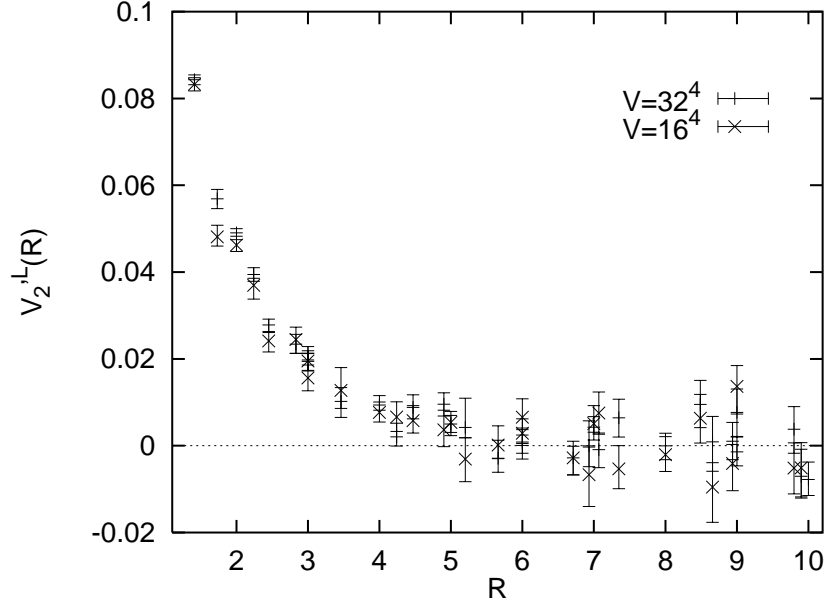


FIG. 11. Comparison between $\tilde{V}_2^L(R)$ at $\beta = 2.74$ obtained on a 16^4 lattice and a 32^4 lattice (in lattice units).

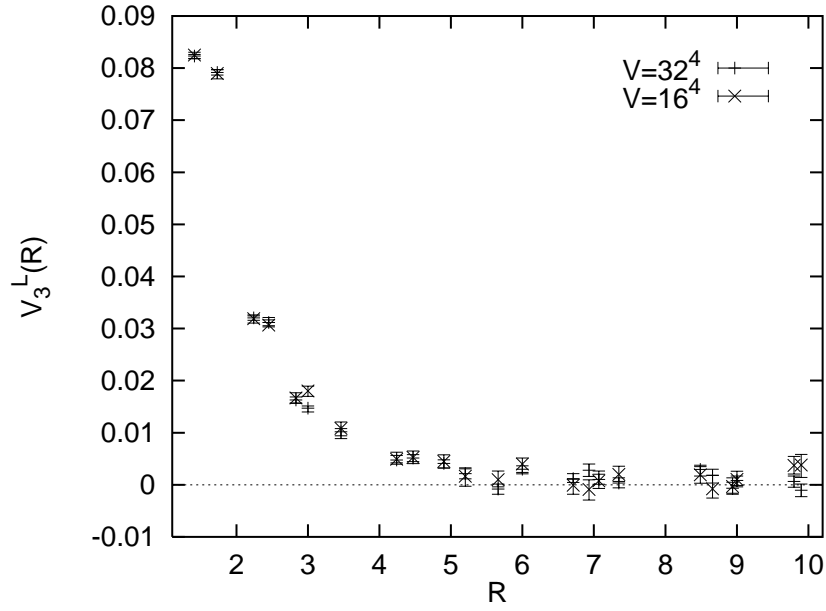


FIG. 12. Comparison between $\tilde{V}_3^L(R)$ at $\beta = 2.74$ obtained on a 16^4 lattice and a 32^4 lattice (in lattice units).

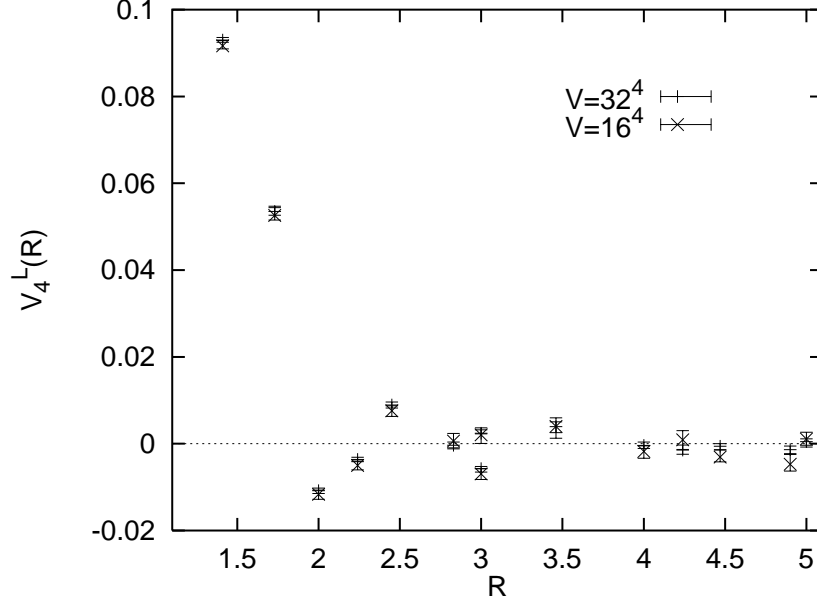


FIG. 13. Comparison between $\tilde{V}_4(R)$ at $\beta = 2.74$ obtained on a 16^4 lattice and a 32^4 lattice (in lattice units).

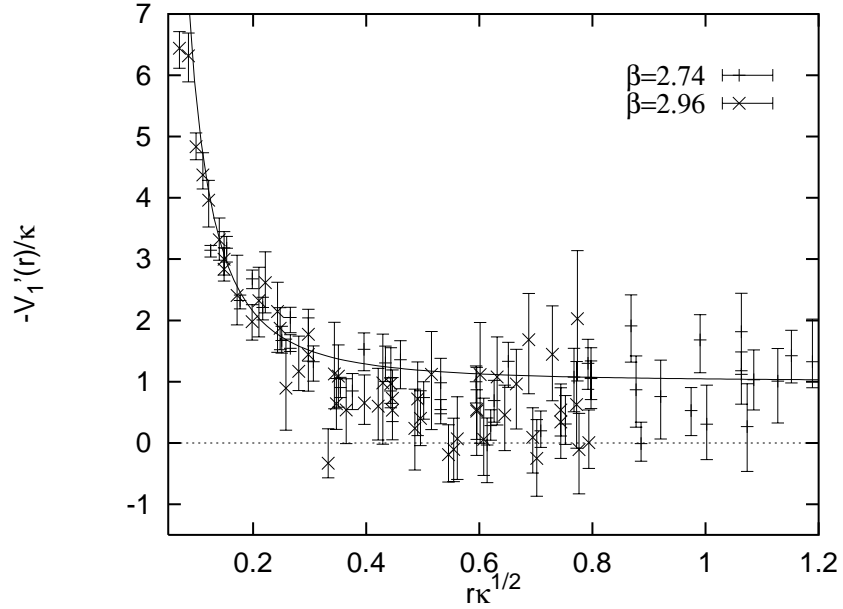


FIG. 14. The spin-orbit potential V_1' , together with a fit curve of the form $-V_1'(r) = \kappa + h/r^2$ (with $h = 0.046$) in units of the string tension.

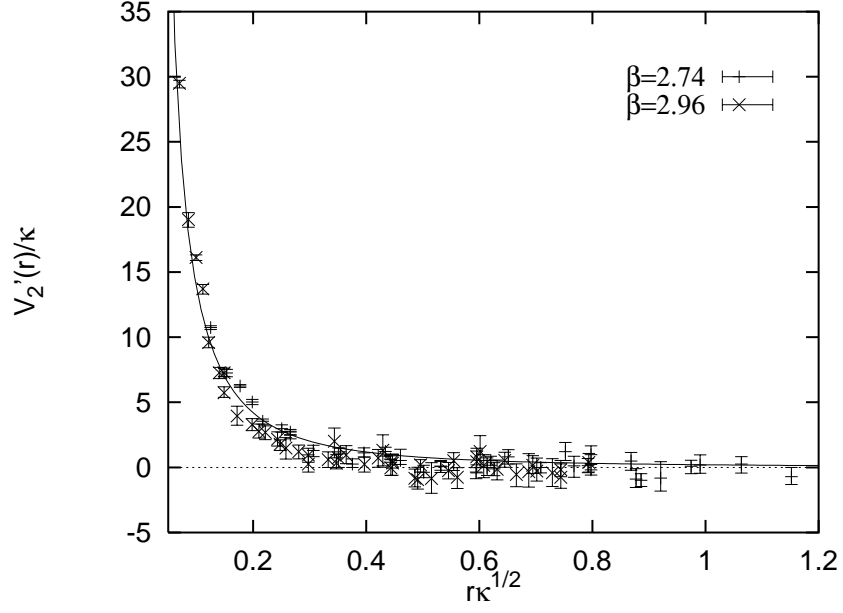


FIG. 15. The spin-orbit potential V_2' in comparison to the continuum expectation from Eq. (53).

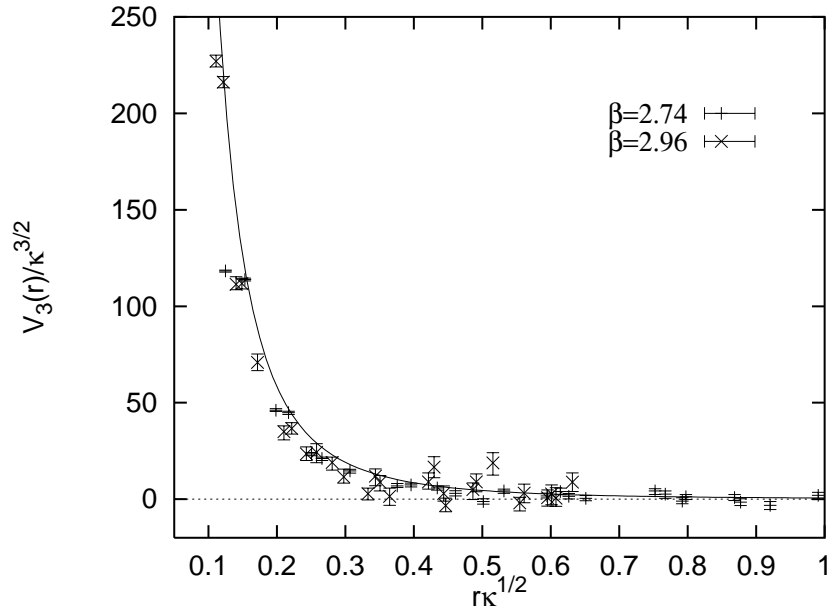


FIG. 16. The spin-spin potential V_3 in comparison to the continuum expectation from Eq. (54).

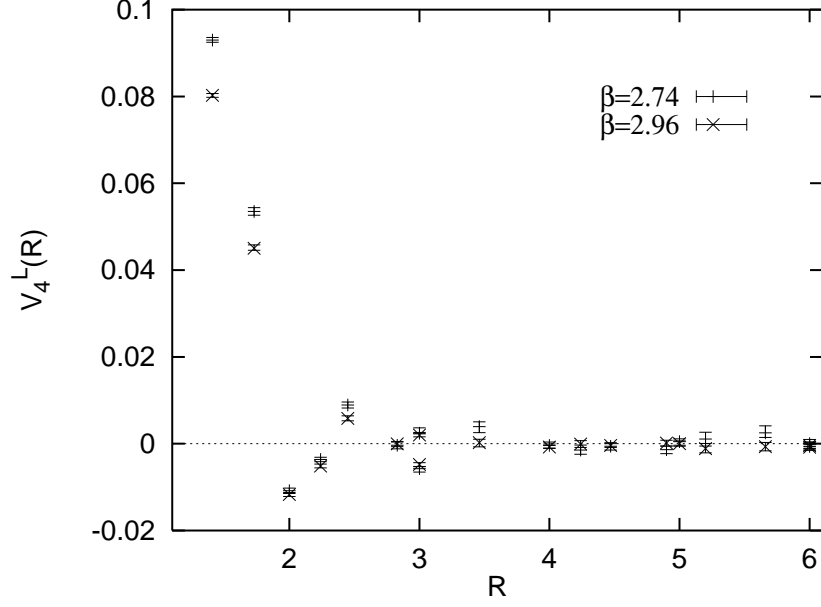


FIG. 17. The spin-spin potential \tilde{V}_4 for the two β -values in lattice units.

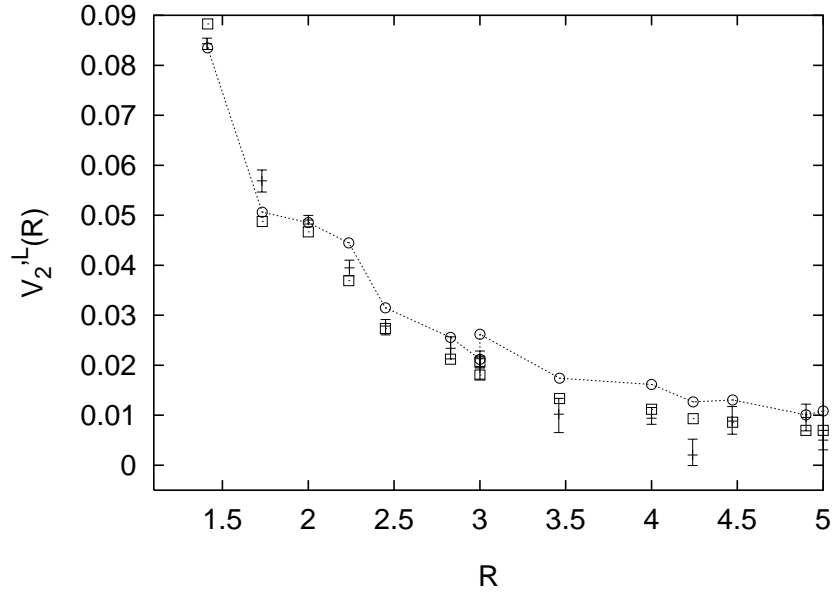


FIG. 18. Comparison of the lattice potential \tilde{V}_2^L (points with error bars) to tree level (open squares) and two loop running coupling improved (open circles) lattice perturbation theory.

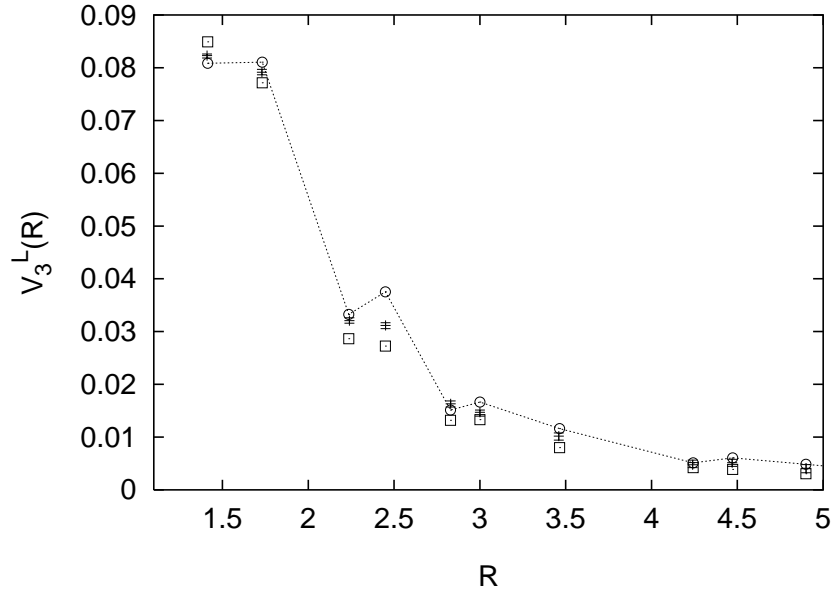


FIG. 19. Same as Fig. 18 for \tilde{V}_3 .

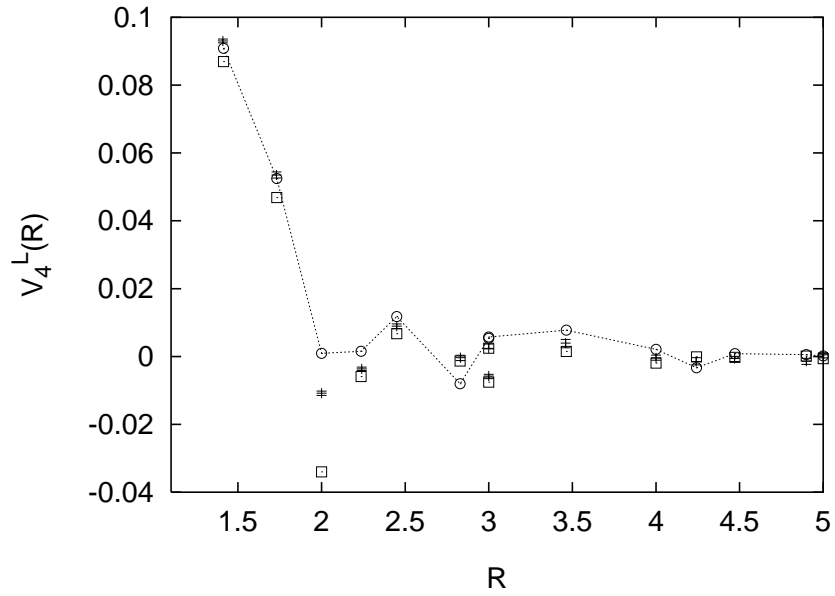


FIG. 20. Same as Fig. 18 for \tilde{V}_4 .